

# Nuclear parton distribution functions with uncertainties in the general mass variable flavor number scheme

Hamzeh Khanpour<sup>1,2</sup> , \* Maryam Soleymaninia<sup>2</sup> , † S. Atashbar  
Tehrani<sup>2</sup> , ‡ Hubert Spiesberger<sup>3</sup> , § and Vadim Guzey<sup>4</sup>  ¶

<sup>(1)</sup> *Department of Physics, University of Science and Technology of Mazandaran, P.O.Box 48518-78195, Behshahr, Iran*

<sup>(2)</sup> *School of Particles and Accelerators, Institute for Research in  
Fundamental Sciences (IPM), P.O.Box 19395-5531, Tehran, Iran*

<sup>3</sup> *PRISMA<sup>+</sup> Cluster of Excellence, Institut für Physik,  
Johannes-Gutenberg-Universität, Staudinger Weg 7, D-55099 Mainz, Germany*

<sup>4</sup> *National Research Center “Kurchatov Institute”,  
Petersburg Nuclear Physics Institute (PNPI), Gatchina 188300, Russia*

(Dated: December 31, 2023)

The aim of this article is to describe a new set of nuclear parton distribution functions (nuclear PDFs) at next-to-leading order (NLO) and next-to-next-to-leading order (NNLO) accuracy in perturbative QCD. The most commonly used nuclear deep-inelastic scattering (DIS) data analyzed in this study are complemented by the available charged-current neutrino DIS experimental data with nuclear targets that are sensitive to the flavor decomposition of non-isoscalar nuclei to obtain a mutually consistent behavior for both up and down valence quarks. This analysis is based on a publicly available open-source tool, **APFEL**, which has been modified to be applicable for our nuclear PDFs analysis. Heavy quark contributions to nuclear DIS are considered within the framework of the **FONLL** general-mass variable-flavor-number scheme. The most recent **CT18** PDFs are used as baseline proton PDFs. The uncertainties of nuclear PDFs are determined using the standard ‘Hessian approach’. The main results of this global QCD analysis are compared with the existing nuclear PDF sets and with the fitted cross-sections. Very good agreement is achieved. The nuclear PDFs presented in this study are available via the standard **LHAPDF** library for applications in high-energy nuclear collisions.

PACS numbers: 12.38.-t, 24.85.+p, 13.15.+g, 13.60.Hb

## CONTENTS

I. Introduction	1	D. Fit quality and comparison of data and theory	18
II. Theoretical formalism and input distributions	2	VI. Summary and conclusions	20
A. The parton distributions of the nucleus	3	Acknowledgments	21
B. Heavy flavor contributions	4	References	24
III. Nuclear DIS datasets	4		
A. Neutral-current lepton-nucleus ( $\ell^\pm A$ ) DIS data	5		
B. Charged-current (anti)neutrino-nucleus ( $\nu A$ ) DIS data	7		
IV. $\chi^2$ minimization and uncertainty estimation	8		
V. Results and discussions	9		
A. Best fit parameters	9		
B. KSASG20 nuclear PDFs and their uncertainties	12		
C. Comparison with other nuclear PDF sets	15		

## I. INTRODUCTION

It is well-known that the nuclear parton distribution functions (nuclear PDFs) [1–19] which quantify the structure of quarks and gluons in bound nucleons is an essential tool for the calculation of hard scattering cross sections in charged-lepton deeply inelastic scattering (DIS) of nuclear targets and high-energy heavy-ion collisions. Based on the collinear factorization theorem, the non-perturbative nuclear PDFs are believed to be process independent, and as for the usual PDFs, their scale dependence is governed by the standard DGLAP evolution equations [20–23]. These assumptions have been shown to be consistent with nuclear DIS experimental data, and with data from heavy-ion collisions at the CERN-LHC.

A precise determination of nuclear PDFs is crucial for studies of the strong interaction in high-energy scattering

\* [Hamzeh.Khanpour@cern.ch](mailto:Hamzeh.Khanpour@cern.ch)

† [Maryam\\_Soleymaninia@ipm.ir](mailto:Maryam_Soleymaninia@ipm.ir)

‡ [Atashbar@ipm.ir](mailto:Atashbar@ipm.ir)

§ [spiesber@uni-mainz.de](mailto:spiesber@uni-mainz.de)

¶ [guzey\\_va@nrcki.pnpi.ru](mailto:guzey_va@nrcki.pnpi.ru)

processes in heavy-ion collisions, such as proton-lead (p-Pb) and lead-lead (Pb-Pb) collisions at the CERN-LHC. Furthermore, nuclear PDFs are important ingredients for the calculation of cross sections in neutrino interactions with heavy nuclear targets,  $\nu N$ . The high-energy interaction of neutrinos with nuclear targets is sensitive to the separation of up- and down-type quarks, and hence, could provide very important information for the decomposition of quark flavors in a QCD analysis [4].

Several collaborations have recently presented new determinations of the nuclear PDFs using the available experimental data, improved theoretical assumptions and advanced methodological settings. For the most recent determination of nuclear PDFs, we refer the reader to the analyses by the nNNPDF Collaboration [1, 2], KA15 [3], EPPS16 [5], TUJU19 [4], RKPZ [7], AT12 [10], KP14 [11], DSSZ [12], HKN07 [17] and nCTEQ15 [18]. Some of the mentioned nuclear PDF determinations are based on nuclear DIS data only. By using these data alone with a rather limited kinematic coverage, significant simplifying assumptions for the nuclear PDF parameterizations need to be taken into account. Hence, the constraints on the extracted quark and gluon nuclear PDFs are weak in these analyses.

Nuclear PDFs at NNLO accuracy in pQCD have been studied for the first time by KA15 [3], in the zero-mass variable-flavor-number scheme (ZM-VFNS). In addition, the more recent work by nNNPDF1.0 [1] is also performed at NNLO, applying the NNPDF methodology, and the resulting nuclear PDFs are determined by a Neural Network (NN) in the general-mass variable-flavor-number scheme (GM-VFNS). Also the most recent study by TUJU19 [4] is performed at NNLO accuracy, based on the open-source xFitter package [24] within the nCTEQ framework.

It is interesting to do the same study considering the different framework and define the bound nucleus PDFs relative to a free nucleon baseline using the most recent proton PDF determination. The work presented in this paper focuses on the determination of new nuclear PDF sets, which we refer to as KSASG20, at NLO and NNLO accuracy in pQCD. All available and up-to-date neutral current charged-lepton nuclear DIS and charged-current neutrino DIS experimental data are used. The former is sensitive to the flavor decomposition of non-isoscalar nuclei. It will be very interesting to repeat the analysis described here and determine a new set of nuclear PDFs by adding the data from proton-lead collisions at the LHC [25–29]. This is left for future work. The work presented in this paper is based on the publicly available open-source APFEL package [30] which has been modified in order to accommodate the data from nuclear collisions, i.e. neutral current charged-lepton nuclear DIS and charged-current neutrino DIS on nuclear targets. For the heavy-quark contributions to nuclear DIS, we consider the FONLL-B and FONLL-C GM-VFNS for our NLO and NNLO analyses, respectively. The standard ‘Hessian’ approach is used to estimate the uncertainties of

nuclear PDFs for quarks and gluons due to experimental errors. The resulting uncertainties are examined in view of the sparse kinematic coverage of the available data.

For the free proton baseline, we use the most recent PDF analysis by CT18 [31] which is based mainly on the most recent measurements from the LHC and a variety of available world collider data. The CT18 PDFs are consistent with our assumptions and the kinematical cuts made for our nuclear PDF analysis. The nuclear PDFs presented in this study are available via the standard LHAPDF library in order to provide an open-source tool for phenomenological applications.

We should mention here that, in most recent years, a large amount of new and precise data from the LHC in proton-lead and lead-lead collisions became available [25–29]. These high precision data, especially data for  $W$  and  $Z$  boson production in proton-lead collisions from the ATLAS and CMS Collaborations at center-of-mass energies of 5.02 TeV and 8.16 TeV, could provide further constraints to the nuclear PDFs, especially for the case of nuclear gluon PDFs. Their impact on the nuclear PDFs has been extensively studied in Refs. [2, 5] to determine well-constrained quark and gluon densities. In addition, an analysis of the impact of available experimental data in proton-lead collisions from Run I at the LHC on nuclear modifications of PDFs is reported in Ref. [32] where the Bayesian reweighting technique [33–35] was used. In Ref. [36] the impact of the single inclusive  $D^0$  meson production data from LHCb [37] in proton-lead collisions on nuclear PDFs is quantified by the Hessian reweighting method. In terms of future work, we plan to revisit this study and consider also these hadron collider data.

The remainder of the paper is organized as follows: In Sec. II, we briefly review the general theoretical formalism for a global QCD analysis of nuclear PDFs and our assumptions for the input parameterization. This section also describes how we include heavy flavor contributions in the nuclear PDF analysis. The charged lepton-nucleus DIS and the neutrino(antineutrino)-nucleus DIS data analyzed in this study are listed and discussed in Sec. III. Then, in Sec. IV, the procedure of  $\chi^2$  minimization and the estimation of nuclear PDF uncertainties are presented. In Sec. V, we show and discuss in detail the global fit results and compare with other nuclear PDFs available in the literature. This section also includes our discussions of the fit quality and the data-theory comparison. Finally, some discussions and a brief summary of the main results are given in Sec. VI.

## II. THEORETICAL FORMALISM AND INPUT DISTRIBUTIONS

This section presents the theoretical framework used in our analysis. First, we present the parameterization of the KSASG20 parton distributions of the nucleus. Then we discuss our method to include the heavy flavor contributions in the nuclear DIS processes.

### A. The parton distributions of the nucleus

In this section, we present our strategy to parameterize the KSASG20 nuclear PDFs at the input scale. Similar to our previous analysis [3] and as in other QCD analyses available in the literature [15, 17], we will work within the conventional approach which defines the nuclear PDFs,  $x f_i^{p/A}(x, Q_0^2; A, Z)$ , for a bound proton in a nucleus with atomic mass number  $A$  with respect to those for a free proton,  $x f_i^p(x, Q_0^2)$ , through a multiplicative nuclear modification factor,  $\mathcal{W}_i(x, A, Z)$ :

$$x f_i^{p/A}(x, Q_0^2; A, Z) = \mathcal{W}_i(x, A, Z) \times x f_i^p(x, Q_0^2), \quad (1)$$

where  $i$  is an index to distinguish the distribution functions for the valence quarks  $u_v$  and  $d_v$ , the sea-quarks  $\bar{d}$ ,  $\bar{u}$ , the strange quark  $s$  and  $\bar{s}$ , and the gluon  $g$ . In the KSASG20 nuclear PDF analysis, we use for the free proton PDFs the most recent PDF set of CT18 [31] at the input scale  $Q_0^2 = 1.69 \text{ GeV}^2$ , i.e.,

$$x f_i^p(x, Q_0^2) = x f_i^{p, \text{CT18}}(x, Q_0^2). \quad (2)$$

For the nuclear modification functions,  $\mathcal{W}_i(x, A, Z)$ , we exactly follow the QCD analyses described in Refs. [3, 10, 13, 17, 38–40] and assume the following cubic-type modification function,

$$\mathcal{W}_i(x, A, Z) = 1 + \left(1 - \frac{1}{A^\alpha}\right) \times \frac{a_i(A) + b_i x + c_i x^2 + d_i x^3}{(1-x)^{\beta_i}}. \quad (3)$$

An advantage of the cubic form with the additional term  $d_i$  in contrast to a quadratic-type function, i.e. with  $d_i = 0$  is, for example, that the nuclear modification becomes flexible enough to accommodate both shadowing and anti-shadowing in the valence quark distributions. For a detailed investigation of these functions, we refer the reader to Refs. [3, 16, 17].

In general, all the coefficients  $a_i$ ,  $b_i$ ,  $c_i$  and  $d_i$  could carry an  $A$ - and a  $Z$ -dependence [3]. However, experimental data do not provide sufficient information to perform a stable fit for such a general ansatz. We therefore impose the simplifying assumption that only  $a_i$  is  $A$ -dependent. The explicit  $A$ -dependent pre-factor in  $\mathcal{W}_i$  in Eq. (3) is constructed in such a way that for the proton ( $A = 1$ ) one recovers the underlying free proton PDFs. The parameter  $\alpha$  is considered to be fixed at  $\alpha = \frac{1}{3}$ . The two terms of the pre-factor  $1 - A^{-\alpha}$  describe nuclear volume and surface contributions [16, 41]. For the valence quark distributions,  $\beta_v$  is fixed at 0.81, and for the sea quark and gluon densities we fix  $\beta_{\bar{q}} = \beta_g = 1$  [16]. The coefficients  $a_i(A)$  in Eq. (3) depend on the atomic number  $A$ , but not all of them are free parameters that can be fitted. Among them only  $a_{\bar{q}}$  needs to be determined from the QCD fit, while we determine  $a_{u_v}$  and  $a_{d_v}$  for the valence quarks, and  $a_g$  for the gluon, from sum rules. These coefficients are constrained for each atomic number  $A$  and hence, they are different for different nuclei.

There are three constraints for  $a_{u_v}$ ,  $a_{d_v}$  and  $a_g$  due to the sum rules for the nuclear charge  $Z$ , the baryon number  $A$ , and from momentum conservation [3, 17]. The nuclear charge is given by,

$$Z = \int_0^1 dx \frac{A}{3} \left[ 2f_{u_v}^{p/A}(x, Q_0) - f_{d_v}^{p/A}(x, Q_0) \right], \quad (4)$$

The baryon number is expressed as

$$A = \int_0^1 dx \frac{A}{3} \left[ f_{u_v}^{p/A}(x, Q_0) + f_{d_v}^{p/A}(x, Q_0) \right], \quad (5)$$

and finally the momentum sum rule reads

$$\int_0^1 dx \sum_i x f_i^{p/A}(x, Q_0) = 1. \quad (6)$$

We emphasize that, with these prescriptions,  $a_v$  for the valence up- and down-quark are assumed to be different,  $a_{u_v} \neq a_{d_v}$ , and hence, the nuclear correction factors for the valence distributions  $\mathcal{W}_{q_v}(x, A, Z)$  are not the same. However, both weight functions are expected to be very similar in shape. The remaining parameters in Eq. (3) are obtained by a global  $\chi^2$  analysis.

Using the PDFs for a bound proton inside a nucleus, the PDFs for a general nucleus ( $A, Z$ ) can be written as

$$f_i^{(A,Z)}(x, Q^2; A, Z) = \frac{1}{A} \left[ Z f_i^{p/A}(x, Q^2; A, Z) + (A - Z) f_i^{n/A}(x, Q^2; A, Z) \right]. \quad (7)$$

The bound neutron PDFs,  $f_i^{n/A}(x, Q^2; A, Z)$ , are obtained from the bound proton PDFs by assuming isospin symmetry. Hence, for all parton species one can write explicitly:

$$\begin{aligned} f_{u_v}^{(A,Z)}(x, Q_0^2) &= \frac{1}{A} \mathcal{W}_{u_v}(x, A, Z) \left[ Z f_{u_v}(x, Q_0^2) + N f_{d_v}(x, Q_0^2) \right] \\ f_{d_v}^{(A,Z)}(x, Q_0^2) &= \frac{1}{A} \mathcal{W}_{d_v}(x, A, Z) \left[ Z f_{d_v}(x, Q_0^2) + N f_{u_v}(x, Q_0^2) \right] \\ f_{\bar{u}}^{(A,Z)}(x, Q_0^2) &= \frac{1}{A} \mathcal{W}_{\bar{q}}(x, A, Z) \left[ Z f_{\bar{u}}(x, Q_0^2) + N f_{\bar{d}}(x, Q_0^2) \right], \\ f_{\bar{d}}^{(A,Z)}(x, Q_0^2) &= \frac{1}{A} \mathcal{W}_{\bar{q}}(x, A, Z) \left[ Z f_{\bar{d}}(x, Q_0^2) + N f_{\bar{u}}(x, Q_0^2) \right], \\ f_s^{(A,Z)}(x, Q_0^2) &= f_{\bar{s}}^{(A,Z)}(x, Q_0^2) = \mathcal{W}_{\bar{q}}(x, A, Z) f_s(x, Q_0^2), \\ f_g^{(A,Z)}(x, Q_0^2) &= \mathcal{W}_g(x, A, Z) f_g(x, Q_0^2). \end{aligned} \quad (8)$$

Here we have assumed flavor dependent sea-quark densities, i.e.,  $f_{\bar{d}}^{(A,Z)} \neq f_{\bar{u}}^{(A,Z)}$ . The nuclear DIS data which we include in our analysis are not sensitive enough to constrain the sea-quark flavor decomposition, but the neutrino DIS data are nicely sensitive to the separation of up- and down-type quarks [4, 12]. Since we use CT18 as baseline proton PDFs, the strange quark distributions in the nuclei are assumed to be flavor symmetric,  $f_{\bar{s}}^{(A,Z)} = f_s^{(A,Z)}$ . We show that the parametrization presented above is sufficiently flexible to allow a good fit quality to the available datasets.

Nucleus	Experiment	Number of data points	$\chi^2_{\text{NLO}}$	$\chi^2_{\text{NNLO}}$	Reference
$F_2^A/F_2^D$					
He/D	SLAC-E139	18	37.66	36.09	[59]
	NMC-95	16	14.71	14.84	[49]
Li/D	NMC-95	15	22.88	23.24	[49]
Li/D ( $Q^2$ dep.)	NMC-95	153	182.14	188.80	[51]
Be/D	SLAC-E139	17	43.60	41.07	[56]
C/D	EMC-88	9	11.00	11.86	[50]
	EMC-90	2	0.11	0.044	[59]
	SLAC-E139	7	47.01	42.75	[56]
	NMC-95	15	14.97	14.58	[49]
	FNAL-E665	4	10.64	10.26	[64]
	JLAB-E03-103	103	265.39	229.69	[62]
C/D ( $Q^2$ dep.)	NMC-95	164	157.86	163.48	[51]
N/D	BCDMS-85	9	13.72	17.25	[52]
	HERMES-03	92	70.09	84.14	[61]
Al/D	SLAC-E49	18	36.57	31.12	[57]
	SLAC-E139	17	12.91	13.56	[56]
Ca/D	EMC-90	2	1.82	1.61	[59]
	NMC-95	15	57.37	82.57	[49]
	SLAC-E139	7	8.05	9.22	[59]
	FNAL-E665	4	5.01	6.44	[64]
Fe/D	SLAC-E87	14	8.31	6.22	[58]
	SLAC-E139	23	45.65	52.75	[56]
	SLAC-E140	6	28.46	15.20	[60]
	BCDMS-87	10	20.64	21.01	[54]
Cu/D	EMC-93	19	13.00	12.75	[48]
Kr/D	HERMES-03	84	92.81	109.70	[61]
Ag/D	SLAC-E139	7	20.47	19.20	[56]
Sn/D	EMC-88	8	17.88	20.44	[50]
Xe/D	FNAL-E665-92	4	3.30	3.45	[63]
Au/D	SLAC-E139	18	76.17	63.64	[56]
Pb/D	FNAL-E665-95	4	10.64	10.26	[64]
<b>Total</b>		<b>884</b>			

**Table I:** The charged lepton DIS experimental datasets for  $F_2^A/F_2^D$  used in the KSASG20 nuclear PDF analysis. The specific nuclear targets, the experiment, the number of data points, and the related references are listed. The values of  $\chi^2$  for the individual experiment extracted from our NLO and NNLO analysis are shown as well.

### B. Heavy flavor contributions

We note that the correct treatment of heavy quark mass contributions is an important asset of a global PDF analysis. To account for the mass dependence in the KSASG20 nuclear PDF analysis for the charm and bottom PDFs, we treat the heavy quarks within the GM-VFNS. We refer the reader to Refs. [42, 43] for a detailed overview. For the KSASG20 analysis at NLO we use the fixed-order plus next-to-leading log scheme FONLL-B, and for the NNLO analysis the FONLL-C scheme is applied [44, 45]. Both the FONLL-B and FONLL-C schemes are implemented in the public APFEL package [30]. We refer the reader to Ref. [46] for more details of these schemes. In order to remain consistent with the CT18 [31] baseline proton PDF analysis, for both the NLO and the NNLO fits, the heavy-quark masses are fixed at  $m_c = 1.30$  GeV and  $m_b = 4.75$  GeV. The strong coupling constant is set equal to  $\alpha_s(M_Z) = 0.118$  [47] for

both the NLO and the NNLO fits.

### III. NUCLEAR DIS DATASETS

In this section, we discuss in detail the datasets which we have used in the KSASG20 nuclear PDF analysis. First, we start by presenting the neutral-current charged lepton-nucleus ( $\ell^\pm A$ ) DIS data. Then, we discuss the charged-current neutrino(antineutrino) DIS experimental data with nuclear targets which are nicely sensitive to the flavor decomposition of non-isoscalar nuclei. This section also includes a detailed investigation of our data selection and kinematical cuts that need to be made when performing the KSASG20 global QCD analysis.

Nucleus	Experiment	Number of data points	$\chi^2_{\text{NLO}}$	$\chi^2_{\text{NNLO}}$	Reference
$F_2^A/F_2^C$					
Be/C	NMC-96	15	12.97	17.48	[53]
Al/C	NMC-96	15	7.09	6.83	[53]
Ca/C	NMC-96	20	30.33	34.83	[49]
	NMC-96	15	9.98	9.38	[53]
Fe/C	NMC-96	15	12.49	11.97	[53]
Sn/C	NMC-96	144	222.65	215.38	[53]
	NMC-96	15	57.29	51.47	[55]
Pb/C	NMC-96	15	19.66	17.72	[53]
<b>Total</b>		<b>254</b>			
$F_2^A/F_2^{Li}$					
C/Li	NMC-95	20	38.58	39.96	[49]
Ca/Li	NMC-95	20	57.77	74.53	[49]
<b>Total</b>		<b>40</b>			

**Table II:** Same as Table I, but for the charged lepton DIS experimental datasets for  $F_2^A/F_2^C$  and  $F_2^A/F_2^{Li}$ .

Nucleus	Experiment	Number of data points	$\chi^2_{\text{NLO}}$	$\chi^2_{\text{NNLO}}$	Reference
D	NMC-96	126	223.75	84.80	[65]
D	BCDMS	53	58.24	69.73	[66]
D	BCDMS	155	271.55	218.06	[67]
D	HERMES	39	11.05	5.16	[68]
D/p	NMC-96	156	311.69	430.06	[69]
<b>Total</b>		<b>529</b>			

**Table III:** Same as Table I, but for the measurements of the deuteron structure function  $F_2^D$  and deuteron-proton ratio  $F_2^D/F_2^p$ .

### A. Neutral-current lepton-nucleus ( $\ell^\pm A$ ) DIS data

The neutral-current charged lepton-nucleus ( $\ell^\pm A$ ) DIS process is a powerful tool to study the nuclear structure and to extract the nuclear PDFs. Hence, we consider the nuclear DIS data in the analysis as a baseline. The DIS of charged-leptons off nuclear targets which initiated all studies of nuclear PDFs provide the best constraints on nuclear modifications of the quark densities. These data are usually presented as a ratio of structure functions for two different nuclei and span the range from 0.005 to 0.95 in momentum fraction  $x$  with a maximum photon virtuality of  $Q_{\text{max}}^2 = 123 \text{ GeV}^2$ . The nuclear DIS data at lower momentum fractions, namely  $x < 0.01$ , are sensitive to the nuclear modifications of sea quarks,  $\mathcal{W}_{\bar{q}}$ . The data at medium-to-large  $x$  mainly probe the valence quark densities. A separation between the quarks and antiquarks is not possible with these data alone. Other available data such as Drell-Yan (DY) dilepton production and (anti)neutrino collisions off nuclear targets should be used to provide a discrimination between the valence and sea quarks.

All available modern inclusive DIS measurements of neutral-current structure functions on nuclear targets are considered in our KSASG20 analysis. In particular, we use the nuclear DIS data from the NMC, EMC,

and BCDMS experiments at CERN [48–55], measurements from SLAC [56–60], HERMES measurements at HERA [61], as well as JLAB [62] data, and data from the E665 experiment at the Fermilab [63, 64]. The measurements of the nuclear structure functions in such experiments typically are presented as ratios of two different nuclei, given by

$$R(x, Q^2; A_1, A_2) = \frac{F_2(x, Q^2; A_1)}{F_2(x, Q^2; A_2)}. \quad (9)$$

In Tables I and II, the measured nuclear targets used in our KSASG20 QCD analysis are listed. For each dataset, we indicate the nuclei  $A_1$  and  $A_2$  which are used to construct the above structure function ratios. In addition, the experiments, the corresponding number of data points after cut, and the published references are shown as well. In order to judge the quality of the fits, the values of  $\chi^2$  extracted from our NLO and NNLO analyses are also presented. As can be seen from Tables I and II, the number of available data points varies for different nuclei. A very large number of data points is available for the deuteron (Table I) and for heavier nuclei, such as carbon (Table II). For other nuclei, such as e.g. lithium, only a few data points are available (Table II).

In order to remain consistent with the CT18 [31] baseline proton PDF analysis, we consider a kinematical cut

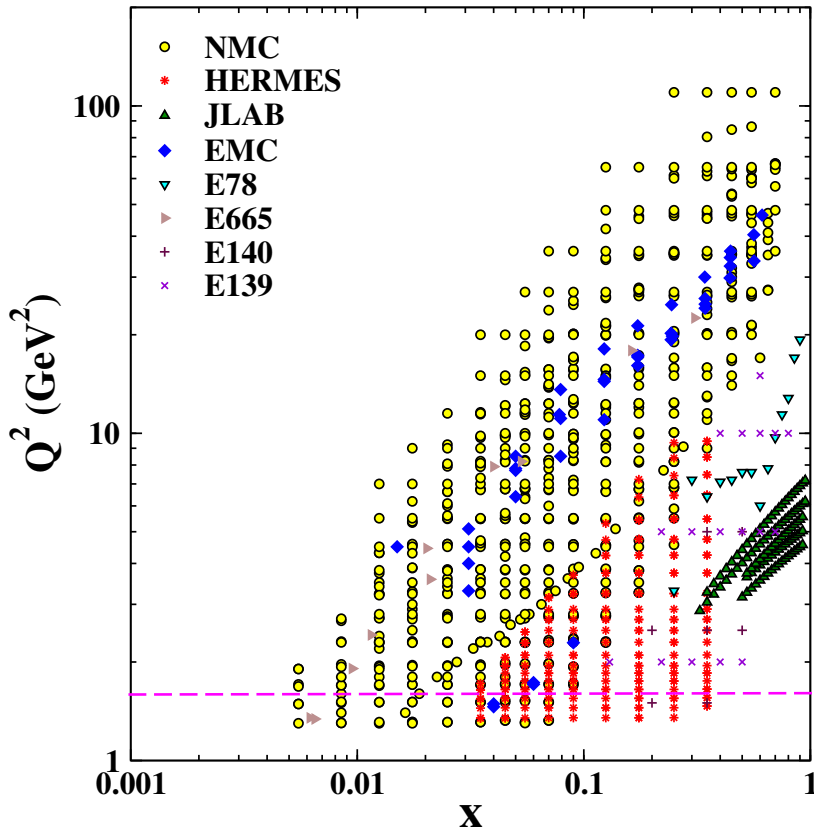


**Figure 1:** The kinematic coverage of the world data for nuclear DIS data used in the present global QCD analysis. The kinematic cut which we apply in our fit is illustrated by the dashed line in the plot.

Nucleus	Experiment	Number of data points	$\chi^2_{\text{NLO}}$	$\chi^2_{\text{NNLO}}$	Reference
$\nu$ Pb	CHORUS	532	455.82	510.25	[71]
$\bar{\nu}$ Pb	CHORUS	532	565.15	544.95	[71]
$\nu$ Fe	CDHSW	698	798.76	716.78	[70]
$\bar{\nu}$ Fe	CDHSW	696	691.67	679.37	[70]
<b>Total</b>		<b>2458</b>			

**Table IV:** The charged-current (anti)neutrino-nucleus ( $\nu A$ ) DIS data used in the KSASG20 analysis. The specific nuclear target, the experiment, the number of data points, the values of  $\chi^2$  extracted from our NLO and NNLO fits, and the related references are listed.

on the momentum transfer  $Q^2$ :

$$Q^2 \geq Q^2_{\text{min}} = 1.69 \text{ GeV}^2. \quad (10)$$

Our choice for the cut on  $Q^2$  is the same as that of the EPS09 [15] and EPPS16 [5] nuclear PDF analyses, where they set  $Q > m_c = 1.3 \text{ GeV}$ . We do not impose any cut on the invariant square of the final state mass,  $W^2$ , again in agreement with what was done in Refs. [5, 15]. After imposing the kinematical cut on  $Q^2$  as presented in Eq. (10), we end up with a total of  $N_{\text{data}} = 1178$  data points for the inclusive DIS measurements of neutral-current struc-

ture functions on nuclear targets. As one can see from Table I, a large amount of these points correspond to the ratios of heavy nuclei with respect to deuterium.

In this work, we treat the deuteron as a nucleus in our fitting procedure. Hence, in addition to the nuclear DIS data discussed above, our analysis also includes the deuteron structure function  $F_2^D$  measurements from NMC [65], BCDMS [66, 67], HERMES [68], and finally the data for the deuteron-proton ratio  $F_2^D/F_2^p$  from NMC [69]. The deuteron data help to extract information on the flavor asymmetric antiquark distributions,

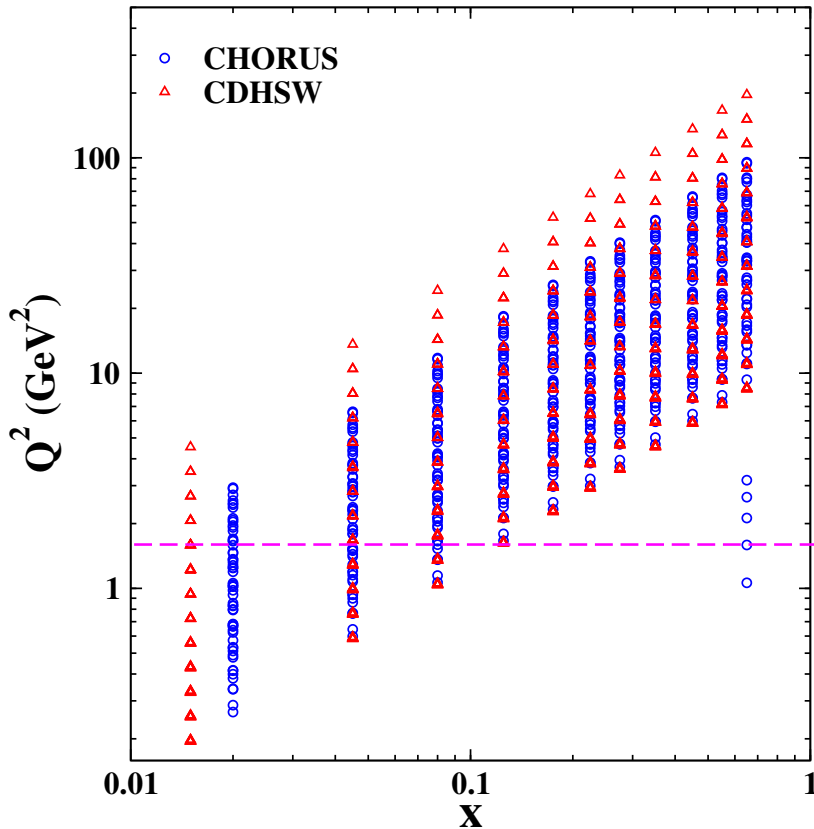


**Figure 2:** The kinematic coverage of the neutrino DIS data used in the present global QCD analysis. Data points lying below the dashed line in the plot are excluded from our fit.

$\bar{d} \neq \bar{u}$ . Therefore, these data are essential for a successful QCD fit and for extracting information on the modification factors for the deuteron. For these specific datasets, a  $Q^2 \geq 2 \text{ GeV}^2$  cut on the momentum transfer is considered. In Table III, we list the measured deuteron structure function  $F_2^D$  and deuteron-proton ratio  $F_2^D/F_2^p$  used in the KSASG20 QCD analysis. After the cuts are applied, 529 data points remain, i.e. 373 for  $F_2^D$  and 156 for  $F_2^D/F_2^p$ .

The kinematic coverage of the world data for nuclear DIS used in the present global QCD analysis is shown in Fig. 1 for some selected experiments. The applied kinematic cut on nuclear DIS data is illustrated by the dashed line in the plot. The data points lying below the line are excluded in the present QCD analysis.

### B. Charged-current (anti)neutrino-nucleus ( $\nu A$ ) DIS data

In addition to neutral-current DIS of charged leptons, we also include the data from neutrino-nucleus charged-current DIS experiments. Including the neutrino-nucleus

DIS data in the analysis improves the nuclear PDF determination because it has additional sensitivity to the flavor decomposition of the PDFs due to the different couplings to down- and up-type quarks [4]. Hence, the nuclear DIS data analyzed in this study are complemented by the available neutrino DIS experimental data in order to achieve well-determined sea-quark densities.

In the KSASG20 nuclear PDF analysis, the cross section measurements from the CDHSW  $\nu$  and  $\bar{\nu}$  Fe experiment [70], and the CHORUS  $\nu$  and  $\bar{\nu}$  Pb experiment [71] have been included. These datasets were included in the analysis by using the measured cross sections for neutrino and antineutrino on iron and lead targets. In the single- $W$  exchange approximation, the cross section for neutrino collisions with nuclear targets can be given by

$$\frac{d^2\sigma}{dx dy} = \mathcal{N} \left[ \frac{y^2}{2} 2xF_1^m + \left( 1 - y - \frac{M_N xy}{2E_\nu} \right) F_2^m \pm y \left( 1 - \frac{1}{y} \right) xF_3^m \right], \quad (11)$$

where  $x$  and  $y$  are the standard kinematical variables for a DIS process, and  $m = \nu$  and  $\bar{\nu}$ . The coupling factor  $\mathcal{N}$

for the (anti)neutrinos-nucleus collision can be written as

$$\mathcal{N} = \frac{G_F^2 M_N E_\nu}{\pi \left(1 + \frac{Q^2}{M_W^2}\right)^2}. \quad (12)$$

The cross section in Eq. (11) is described in terms of three structure functions, namely  $F_1$ ,  $F_2$ , and  $x F_3$ .

The structure functions for neutrino scattering in Eq. (11) are given at leading order (LO) by [4, 12, 47],

$$\begin{aligned} F_2^{\nu A} &\simeq (d^A + s^A + b^A + \bar{u}^A + \bar{c}^A), \\ F_3^{\nu A} &\simeq (d^A + s^A + b^A - \bar{u}^A - \bar{c}^A), \end{aligned} \quad (13)$$

and for antineutrino scattering by

$$\begin{aligned} F_2^{\bar{\nu} A} &\simeq (u^A + c^A + \bar{d}^A + \bar{s}^A + \bar{b}^A), \\ F_3^{\bar{\nu} A} &\simeq (u^A + c^A - \bar{d}^A - \bar{s}^A - \bar{b}^A). \end{aligned} \quad (14)$$

As can be seen from Eqs. (13) and (14),  $F_2$  is proportional to the total singlet combination of quark and anti-quark densities. Hence, it is sensitive to both valence and sea quark densities. In addition,  $F_3$  provides additional sensitivity to the flavor decomposition since it depends on a different linear combination of quark and antiquark PDFs. By combining the nuclear and neutrino DIS data, one can arrive at a considerably improved valence and sea quark separation in the entire region of  $x$  where the data overlap.

In addition to the CDHSW and CHORUS neutrino DIS data, there are more neutrino scattering datasets available in the literature, namely the measured cross sections with an iron target by the NuTeV Collaboration [72], and also the data from the CCFRR Neutrino Collaboration [73]. For the CCFRR measurements, the quantities  $Q^2$  and  $x$  were not publicly available for the cross sections. In addition, only the averaged structure functions  $F_2$  and  $x F_3$  for neutrino and anti-neutrino scattering on iron nuclei are available, which have less sensitivity to the flavor decomposition [4]. Hence, we do not consider the CCFRR data in our analysis.

Several studies in the literature have found some unresolved tension between the NuTeV measurements and the lepton-nucleus data [74, 75]. A similar tension was also reported in Refs. [14, 76] when taking into account the neutrino DIS data from the CHORUS and CCFRR measurements. Detailed studies presented in Refs. [34, 77] have shown that the tension with other data was specifically due to the inclusion of data from the NuTeV experiment. Due to this unresolved tension, we have excluded the NuTeV neutrino DIS data from our QCD analysis.

The charged-current (anti)neutrino-nucleus ( $\nu A$ ) DIS data used in the KSASG20 analysis are presented in Table IV. The number of data points, the respective reference and the specific nuclear target are listed as well. These datasets are subject to the same standard cut as presented in Eq. (10). In total, we include 2458 data points from neutrino-nucleus collisions at CHORUS and CDHSW. The  $\chi^2$  values obtained in our NLO and NNLO fits are shown as well.

Figure 2 shows the kinematic coverage of the data for neutrino and antineutrino DIS from the CDHSW and CHORUS experiments used in the present global QCD analysis. Our kinematic cut applied on neutrino DIS data is illustrated by the dashed line in the plot. The data points lying below the line are excluded in the present QCD analysis.

#### IV. $\chi^2$ MINIMIZATION AND UNCERTAINTY ESTIMATION

The optimal values for the nuclear PDF parameters defined in Eq. (8) are extracted from the nuclear and neutrino DIS data using the global function  $\chi_{\text{global}}^2(\{\xi_i\})$  given by

$$\chi_{\text{global}}^2(\{\xi_i\}) = \sum_{m=1}^{m^{\text{exp}}} w_m \chi_m^2(\{\xi_i\}), \quad (15)$$

where  $m$  labels the experiment.  $w_m$  allows us, in principle, to include datasets with different weight factors. However, we always use the default value  $w_m = 1$  for all experimental datasets [78, 79]. Each experiment contributes with  $\chi_m^2(\{\xi_i\})$  to the global  $\chi^2$ . These terms depend on the fit parameters ( $\{\xi_i\}$ ), which are identified with the parameters of the bound proton PDFs at the initial scale.  $\chi_m^2(\{\xi_i\})$  is calculated as

$$\chi_m^2(\{\xi_i\}) = \left(\frac{1 - \mathcal{N}_m}{\Delta \mathcal{N}_m}\right)^2 + \sum_{j=1}^{N_m^{\text{data}}} \left(\frac{(\mathcal{N}_m \mathcal{O}_j^{\text{data}} - \mathcal{T}_j^{\text{theory}}(\{\xi_i\}))^2}{\mathcal{N}_m \Delta_j^{\text{data}}}\right). \quad (16)$$

Here  $j$  runs over data points,  $m$  indicates a given individual experimental dataset, and  $N_m^{\text{data}}$  corresponds to the total number of data points in this set. In the above equation,  $\mathcal{O}_j^{\text{data}}$  is the value of the measured data point for a given observable, and  $\Delta_j^{\text{data}}$  is the experimental error calculated from the statistical and systematic errors added in quadrature. The theoretical predictions for each data point  $j$  are represented by  $\mathcal{T}_j^{\text{theory}}(\{\xi_i\})$ , which has to be calculated at the same experimental kinematic point  $x$  and  $Q^2$  using the DGLAP-evolved nuclear PDFs with given parameters ( $\{\xi_i\}$ ). We use the CERN subroutine MINUIT [80] to determine the independent fit parameters of nuclear PDFs  $f_i^{(A,Z)}(x, Q^2; A, Z)$  by minimizing  $\chi_{\text{global}}^2(\{\xi_i\})$ .

In Eq. (16),  $\Delta \mathcal{N}_m$  describes the overall normalization uncertainty for each charged lepton DIS experiment. We include the normalization  $\mathcal{N}_m$  of different experiments as a free parameter along with other independent fit parameters ( $\{\xi_i\}$ ). Their values found in a first global fit are kept fixed when we determine the uncertainties of the nuclear PDF parameters.

The quality of the QCD fit can be estimated from the resulting  $\chi^2/N^{\text{data}}$ , where  $N^{\text{data}}$  indicates the number of data points.

After describing the method to obtain the central value of the KSASG20 nuclear PDFs by minimizing the  $\chi_{\text{global}}^2(\{\xi_i\})$  function, we are in a position to present our method to estimate the uncertainties of our nuclear PDFs. There are three established methods, namely the Hessian method [81, 82], the Monte Carlo (MC) method [1, 83] and Lagrange multiplier method [79], which can be used for the error analysis. The analysis of the uncertainties in KSASG20 is done using the standard 'Hessian' approach [5, 43, 81, 82], which we will briefly describe in the following. For the uncertainty estimate, we follow the notation adopted in Refs. [81, 82] and refer the reader to these publications for a detailed discussion of the Hessian formalism.

The KSASG20 nuclear PDF uncertainties are estimated by using the Hessian matrix

$$\left[ \delta f^{(A,Z)} \right]^2 = T^2 \sum_{m,n} \left( \frac{\partial f^{(A,Z)}(x, \{\xi\})}{\partial \xi_m} \right)_{\xi=\hat{\xi}} H_{mn}^{-1} \left( \frac{\partial f^{(A,Z)}(x, \{\xi\})}{\partial \xi_n} \right)_{\xi=\hat{\xi}}, \quad (17)$$

where  $H_{mn}$  corresponds to the components of the Hessian matrix obtained by the CERN subroutine MINUIT,  $\{\hat{\xi}\}$  indicates the set of optimum independent fit parameters, and  $\xi_n$  are the fit parameters of the chosen functional form at the initial scale. The value of  $T^2 = \Delta\chi_{\text{global}}^2$  in Eq. (17) is the tolerance for the required confidence interval. It is calculated so that the confidence level (CL) becomes the one- $\sigma$  error range, i.e. 68% CL, for a given number of independent fit parameters. In an ideal case, with the standard 'parameter-fitting' criterion, one would choose the tolerance criterion  $T^2 = \Delta\chi_{\text{global}}^2 = 1$  for the 68%, i.e. one-sigma CL limit, or  $T^2 = 2.71$  for the 90% CL limit [43]. In the KSASG20 nuclear PDF analysis, the tolerance for  $\chi_{\text{global}}^2$  is based on the method presented in Refs. [5, 17, 43]. In our study with 9 free fit parameters it becomes  $\chi_{\text{global}}^2 = 10$  at the 68% CL.

## V. RESULTS AND DISCUSSIONS

In the following section we present the main results and findings of our QCD analysis. We first discuss the main features of the KSASG20 nuclear PDF parameters. Then, we assess the stability of our NLO and NNLO results with respect to the perturbative order. We present a detailed comparison with the recent NLO and NNLO nuclear PDF analyses available in the literature. Finally, the section is concluded with a discussion of the quality of our fit results by comparing the resulting structure function ratios with the nuclear DIS experimental data, and compare our theoretical predictions with the neutrino DIS data as well.

**Table V:** Best fit parameters and their errors obtained in KSASG20 QCD fits at NLO and NNLO accuracy and at the initial scale  $Q_0^2 = 1.69 \text{ GeV}^2$ . Values marked with (\*) are fixed in our fit since the analyzed nuclear and neutrino DIS data do not constrain these parameters well enough.

Parameters	NLO	NNLO
$a_v$	see Table. VI	see Table. VII
$b_v$	$0.633 \pm 0.034$	$0.464 \pm 0.037$
$c_v$	$-2.594 \pm 0.079$	$-2.163 \pm 0.084$
$d_v$	$2.210 \pm 0.054$	$1.956 \pm 0.056$
$\beta_v$	$0.81^*$	$0.81^*$
$a_{\bar{q}}$	$-0.260 \pm 0.010$	$-0.228 \pm 0.010$
$b_{\bar{q}}$	$5.018 \pm 0.267$	$5.022 \pm 0.308$
$c_{\bar{q}}$	$-22.545 \pm 1.641$	$-21.967 \pm 1.963$
$d_{\bar{q}}$	$30.232 \pm 2.669$	$31.791 \pm 3.498$
$\beta_{\bar{q}}$	$1.0^*$	$1.0^*$
$a_g$	see Table. VI	see Table. VII
$b_g$	$1.790 \pm 0.963$	$4.950 \pm 0.768$
$c_g$	$1.879 \pm 1.717$	$-3.163 \pm 1.104$
$d_g$	$0.0^*$	$0.0^*$
$\beta_g$	$1.0^*$	$1.0^*$
$\alpha_s(M_Z^2)$	$0.118^*$	$0.118^*$
$m_c$	$1.30^*$	$1.30^*$
$m_b$	$4.75^*$	$4.75^*$
$\chi^2/\text{d.o.f}$	$5202.53/4156 = 1.25$	$5090.91/4156 = 1.22$

**Table VI:** Obtained values for the parameters  $a_{u_v}$ ,  $a_{d_v}$ , and  $a_g$  for several nuclei analyzed in this study at NLO accuracy. These parameters are obtained using the sum rules for the nuclear charge  $Z$  and the baryon number  $A$ , and momentum conservation. See Sec. II A for details.

Nucleus	$a_{u_v}$	$a_{d_v}$	$a_g$
$^2\text{D}$	-0.0153058	-0.0153058	-0.406803
$^4\text{He}$	-0.0153058	-0.0153058	-0.406803
$^7\text{Li}$	-0.0156358	-0.0150073	-0.406809
$^9\text{Be}$	-0.0155595	-0.0150711	-0.406806
$^{12}\text{C}$	-0.0153058	-0.0153058	-0.406803
$^{14}\text{N}$	-0.0153058	-0.0153058	-0.406803
$^{27}\text{Al}$	-0.0153881	-0.0152255	-0.406804
$^{40}\text{Ca}$	-0.0153058	-0.0153058	-0.406803
$^{56}\text{Fe}$	-0.0154665	-0.0151529	-0.406805
$^{63}\text{Cu}$	-0.0154849	-0.0151363	-0.406805
$^{84}\text{Kr}$	-0.0156358	-0.0150073	-0.406809
$^{108}\text{Ag}$	-0.0156038	-0.0150337	-0.406808
$^{119}\text{Sn}$	-0.0156417	-0.0150024	-0.406809
$^{131}\text{Xe}$	-0.0157163	-0.0149429	-0.406811
$^{197}\text{Au}$	-0.0157726	-0.0148996	-0.406813
$^{208}\text{Pb}$	-0.0158072	-0.0148737	-0.406815

### A. Best fit parameters

In this work, we analyze nuclear PDFs using the CT18 proton PDF set as a baseline [31]. The nuclear modification factors in Eq. (3) are extracted from QCD fits to the nuclear and neutrino(antineutrino) DIS data. Our best

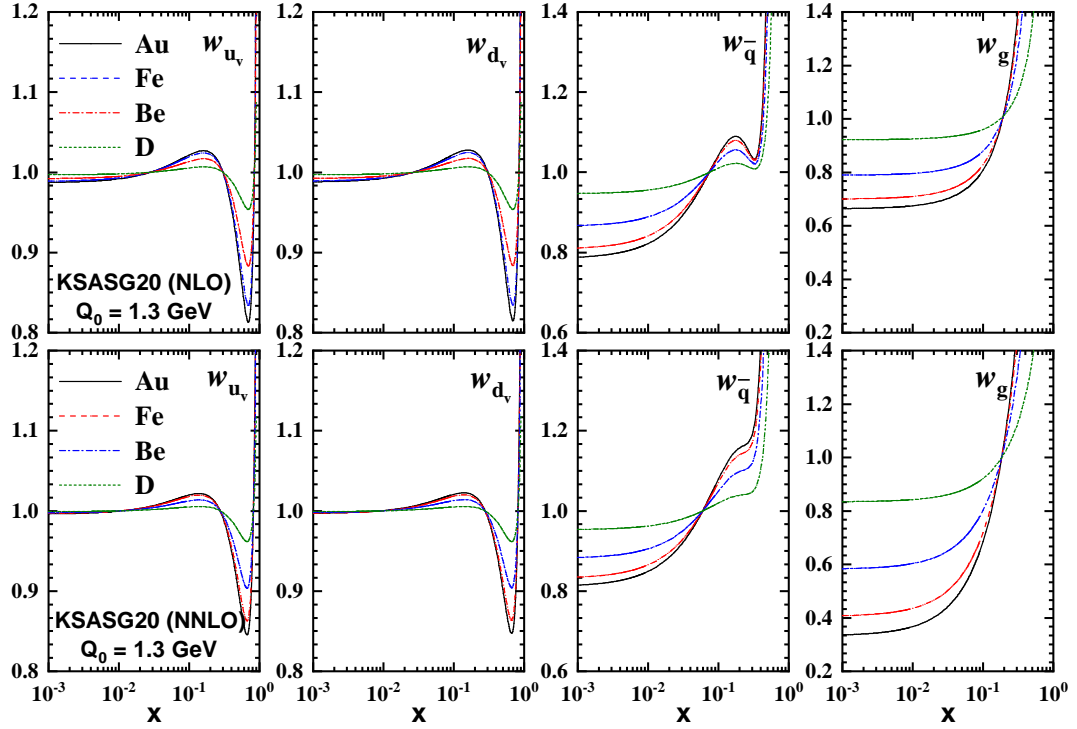


**Figure 3:** The nuclear modification factors defined as ratios of proton PDFs bound in deuterium (D), Beryllium (Be), iron (Fe) and gold (Au) to the corresponding free-proton PDFs of CT18 [31] at NLO (top row) and NNLO (bottom row) accuracy in pQCD and at the initial scale  $Q_0 = 1.30$  GeV.

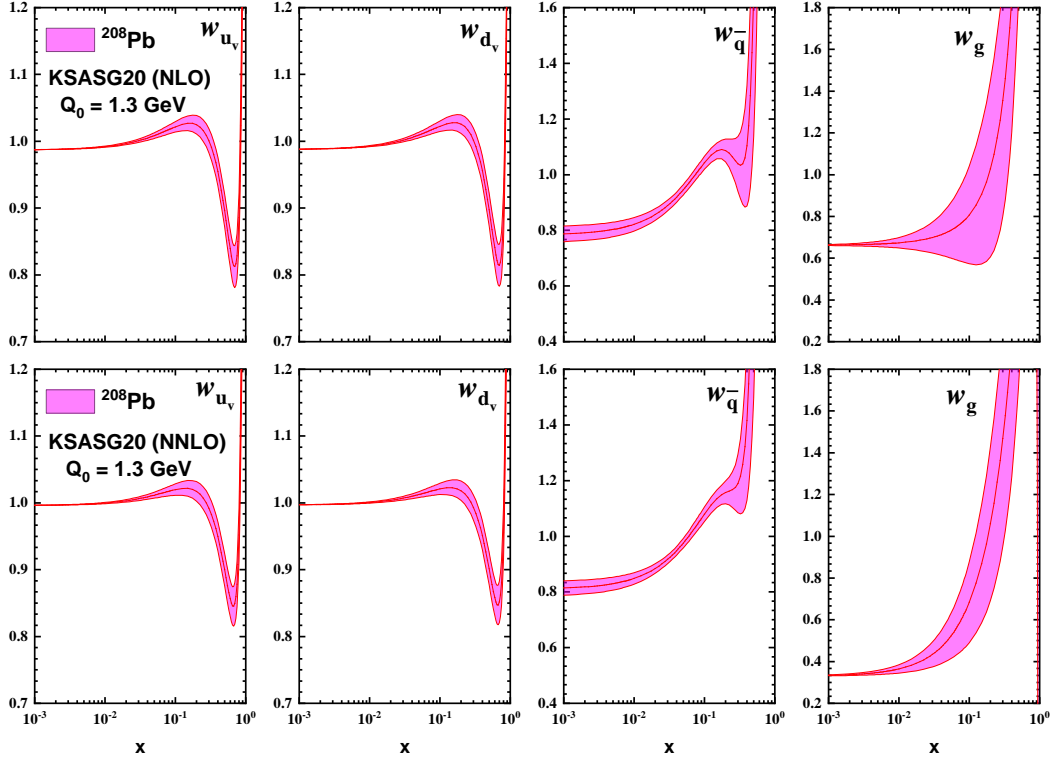


**Figure 4:** The nuclear modification factors defined as ratios of proton PDFs bound in lead to the corresponding free-proton PDFs of CT18 at NLO and NNLO accuracy and at  $Q_0 = 1.3$  GeV. The bands show the 68% uncertainty estimation with  $\Delta\chi^2 = 10$  obtained using the Hessian method.

fit parameters obtained in the KSASG20 NLO and NNLO fits at the initial scale  $Q_0^2 = 1.69$  GeV<sup>2</sup> are presented in Table V along with their errors. Values marked with an asterisk (\*) in this table are fixed at the given particular value since the analyzed nuclear and neutrino DIS data could not constrain these parameters well enough. The fixed values of  $\beta_g = 1$  and  $\beta_{\bar{q}} = 1$  for gluon and sea quarks, as well as the value  $\beta_v = 0.81$  for valence quark densities are motivated by the HKN07 analysis [17]. Freeing these parameters can easily lead to unphysical fit results, and hence, we have decided to keep them fixed at this stage. As we mentioned before, the heavy-quark masses are fixed at  $m_c = 1.30$  GeV and  $m_b = 4.75$  GeV to be consistent with the CT18 proton PDFs. The strong coupling constant is taken as  $\alpha_s(M_Z) = 0.118$  [47].

As discussed in Sec. II A, the nuclear dependent parameters  $a_i(A, Z)$  for the sea quark densities need to be determined from the fit to data. The parameters  $a_i(A, Z)$  for the valence quark and gluon densities depend on the

mass number  $A$  and atomic number  $Z$  in general and are extracted from the three constraints mentioned in Eqs. (4), (5) and (6). The numerical values for these parameters are presented in Tables VI and VII at NLO and NNLO accuracy, respectively.

Regarding the best fit parameters and their errors listed in Table V, some comments are in order. The obtained parameters for the nuclear valence-quark distributions reflect the fact that the nuclear DIS data analyzed in this study constrain these distributions well enough. In addition, neutrino DIS also plays an important role in obtaining a consistent behavior for the up and down valence quarks. As can be seen from Table V, some fit parameters of our sea-quark and gluon densities come with larger errors, especially  $c_g$ . In addition, we fixed  $d_g$  to zero. The nuclear and neutrino DIS data only loosely constrain the gluon nuclear modifications because they cover a too limited range in  $Q^2$ .

To further constrain the nuclear sea-quark and gluon

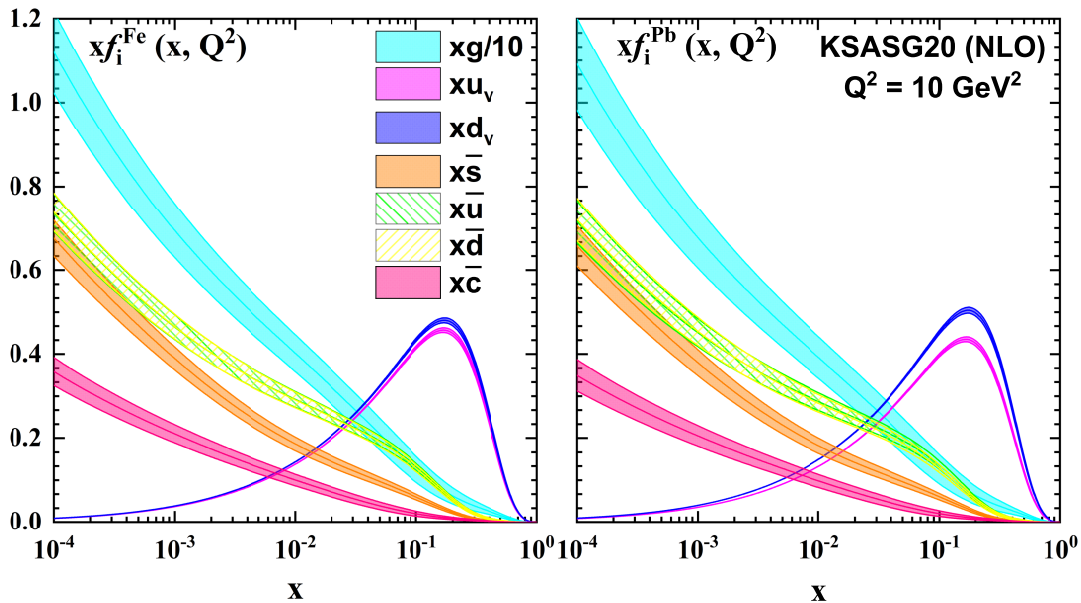


**Figure 5:** KSASG20 nuclear PDFs and their uncertainties at  $Q^2 = 10 \text{ GeV}^2$  for iron (left) and lead (right). The error bands correspond to the uncertainty estimates at 68% CL with  $\Delta\chi^2 = 10$  obtained using the Hessian method.

**Table VII:** Same as Table. VI, but this time at NNLO accuracy.

Nucleus	$a_{u_v}$	$a_{d_v}$	$a_g$
$^2\text{D}$	-0.00428552	-0.00428552	-0.805784
$^4\text{He}$	-0.00428552	-0.00428552	-0.805784
$^7\text{Li}$	-0.00463751	-0.00396711	-0.805789
$^9\text{Be}$	-0.00455612	-0.00403521	-0.805787
$^{12}\text{C}$	-0.00428552	-0.00428552	-0.805784
$^{14}\text{N}$	-0.00428552	-0.00428552	-0.805784
$^{27}\text{Al}$	-0.00437335	-0.00419995	-0.805784
$^{40}\text{Ca}$	-0.00428552	-0.00428552	-0.805784
$^{56}\text{Fe}$	-0.00445710	-0.00412243	-0.805785
$^{63}\text{Cu}$	-0.00447659	-0.00410479	-0.805786
$^{84}\text{Kr}$	-0.00463751	-0.00396711	-0.805789
$^{108}\text{Ag}$	-0.00460337	-0.00399531	-0.805788
$^{119}\text{Sn}$	-0.00468137	-0.00393163	-0.805791
$^{131}\text{Xe}$	-0.00472340	-0.00389841	-0.805792
$^{197}\text{Au}$	-0.00478342	-0.00385224	-0.805794
$^{208}\text{Pb}$	-0.00482028	-0.00382459	-0.805796

densities and reduce their uncertainties, other observables will have to be taken into account. These should include the Drell-Yan data from the Fermilab E772 and E866/NuSea Collaborations [84, 85], from PHENIX and STAR for inclusive pion production in deuteron-gold (d-Au) collisions [86, 87], neutral pion production data from

PHENIX [86], and the charged and neutral pion data from the STAR experiment [87, 88]. Also data from proton-lead (p-Pb) collisions from the ATLAS and CMS Collaborations at the LHC, which have been included in the analyses of nuclear PDFs performed in Refs. [2, 5], are expected to constrain the nuclear gluon density at large momentum fraction. Once more data are included, for example the data from the LHC and a future  $eA$  collider such as LHeC or FCC-he, it should be possible to relax some of the assumptions mentioned above.

## B. KSASG20 nuclear PDFs and their uncertainties

In the following, we discuss the KSASG20 nuclear PDFs including the nuclear modification functions and present a detailed comparison between our NLO and NNLO analyses. We also assess the stability of our NLO and NNLO results with respect to the perturbative order.

In Fig. 3, we show representations of different types of nuclear modification functions for some selected nuclei, deuterium (D), iron (Fe) and gold (Au) at the input scale  $Q_0^2 = 1.69 \text{ GeV}^2$ . The nuclear modification functions are shown for the valence-quark  $\mathcal{W}_{u_v}$  and  $\mathcal{W}_{d_v}$ , sea-quark  $\mathcal{W}_{\bar{q}}$  and gluon  $\mathcal{W}_g$  at NLO (top row) and NNLO (bottom row). We repeat here that, in this work, we have treated the deuterium as a nucleus in the fitting procedure. Hence, as one can see from Fig. 3, small deviations

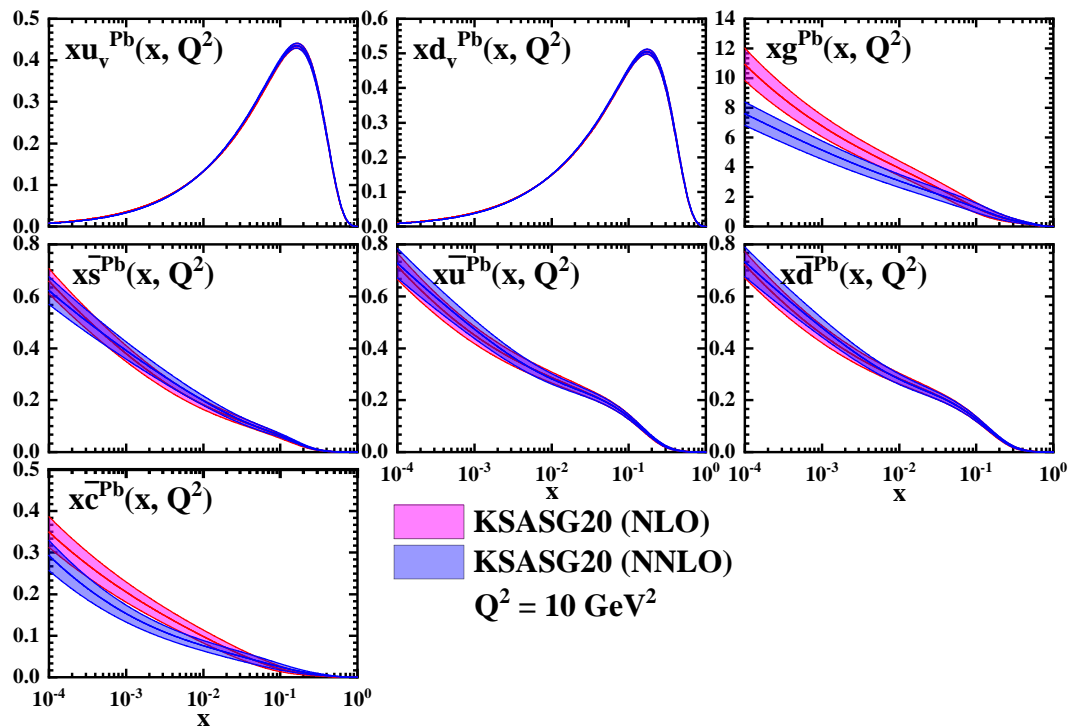


**Figure 6:** Our bound proton PDFs at  $Q^2 = 10 \text{ GeV}^2$  for lead at NLO and NNLO accuracy. The uncertainty bands for the nuclear PDFs have been calculated with  $\Delta\chi^2 = 10$  as described in the text.

from the baseline CT18 proton PDFs are found for the deuterium. The deviations from the CT18 PDFs become larger with increasing atomic mass ( $A$ ), and significant effects are found for the heavier nuclei, such as gold. We should notice here that our results in the small- $x$  region, i.e.  $x < 10^{-2}$ , are not directly constrained by the nuclear and neutrino DIS data, but determined by extrapolation based on our parametrization.

We start our discussion with the nuclear modifications for valence quark densities. As can be seen from Fig. 3, the typical nuclear modification effects, such as anti-shadowing, shadowing and EMC suppression, are visible already at the input scale for the up and down valence quark modifications,  $\mathcal{W}_{u_v}$  and  $\mathcal{W}_{d_v}$ . For the NLO analysis, the nuclear modification for gluon shows a rapid rise with increasing  $x$ ,  $x > 0.1$ . This trend repeats itself for the NNLO analysis, a behavior which is similar to what one can observe in the analyses by HKM01 [16], HKN07 [17] and KA15 [3]. This behavior may be an artifact due to the used parametrization in these analyses. Fig. 3 also shows that for the case of sea-quarks one can observe

the typical nuclear modifications. However, the magnitude of these effects slightly differs at different perturbative orders. Our nuclear modifications for quark and gluon densities are flat in the small- $x$  region. This behavior is similar to the analysis of HKN07 [17] who used the same QCD framework, same assumptions and input parametrization.

We continue with the discussion of the nuclear modification factors and their uncertainties for the case of lead as an example of a large nucleus. Lead is particularly relevant for the present and future heavy-ion program at the LHC for p-Pb and Pb-Pb collisions. The nuclear modification for lead defined as ratios of proton PDFs bound in lead to the corresponding free-proton PDFs (CT18) along with their uncertainties at 68% CL with  $\Delta\chi^2 = 10$  are shown in Fig. 4. The results are shown at the scale  $Q_0 = 1.3 \text{ GeV}$  at NLO and NNLO accuracy. As can be seen, the nuclear modifications for quark and gluon come with relatively large error bands. We should stress here that the uncertainty bands at very small and large  $x$  are not directly constrained by data. Hence, the widening of the

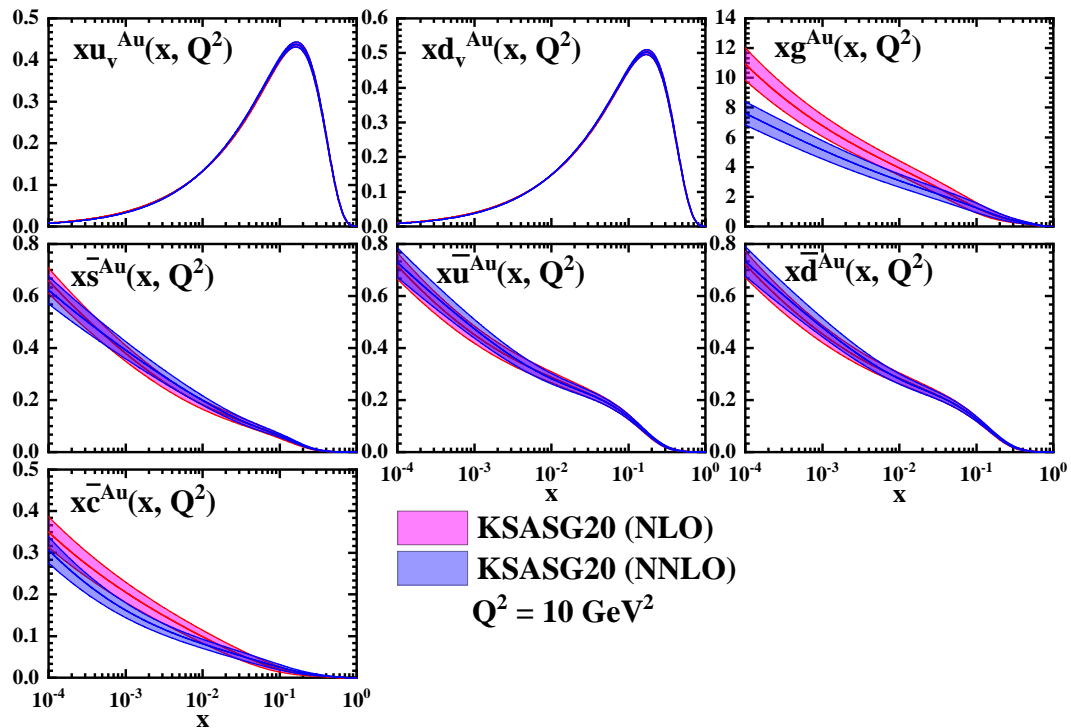


Figure 7: Same as Fig. 6, but for gold.

uncertainty bands results from extrapolating our parameterization into unconstrained kinematic regions.

The resulting nuclear PDFs are presented in Fig. 5 for iron (left) and lead (right), now at  $Q^2 = 10 \text{ GeV}^2$  to show the evolution effects when the PDFs are probed at a typical scale,  $Q^2 > Q_0^2$ . As we mentioned in Sec. II A, the up and down nuclear PDFs have been assumed to be flavor dependent, *i.e.*,  $x\bar{d} \neq x\bar{u}$ . For the strange quark distributions in the nuclei, we assume as usual  $x s = x\bar{s}$ . The perturbatively generated heavy quark densities,  $x\bar{c}$  and  $x\bar{b}$ , are obtained through DGLAP evolution in the FONLL GM-VFNS as implemented in the open-source APFEL package [30]. The uncertainty bands for the nuclear PDFs provided in this study have been calculated using the standard Hessian method with  $\Delta\chi^2 = 10$  as described in Sec. IV. Regarding the KSASG20 nuclear PDFs presented in Fig. 5, several comments are in order. As can be seen, all the gluon and sea-quark densities come with relatively large error bands at small  $x$ , reflecting the fact that there are not enough data constraints below  $x \sim 0.01$ . In our analysis, as can be seen from Eq. (8), we consider flavor asymmetric parameterizations

and allow  $x\bar{u}$  and  $x\bar{d}$  to be different. However, we find only very small differences for the fitted  $\bar{u}$  and  $\bar{d}$  nuclear PDFs; the corresponding error bands shown in Fig. 5 are difficult to distinguish. In our analysis, we fit the strange quark density and consider  $x s = x\bar{s}$ , see Eq. (8), which is consistent with the CT18 free-proton baseline.

In the following, in order to study the perturbative convergence of the nuclear PDFs upon inclusion of higher-order QCD corrections, we compare our NLO and NNLO determinations among each other in terms of shape and uncertainty bands. In Figs. 6 and 7, the NLO and NNLO nuclear PDFs are compared at  $Q^2 = 10 \text{ GeV}^2$  for the valence quark  $xq_v$ , gluon  $xg$ , strange quark  $x\bar{s}$ , sea quarks  $x\bar{u}$  and  $x\bar{d}$ , and finally the perturbatively generated charm quark  $x\bar{c}$  density. It is worth noticing here that the magnitude and the shape of the nuclear PDFs for a given flavor at some arbitrary scale  $Q^2$  depends on the chosen set of reference PDFs for free protons. Due to the limited sensitivity of the analyzed nuclear and neutrino(antineutrino) DIS data to the gluon and sea-quark nuclear PDFs, the provided uncertainty bands are rather large, especially for small values of  $x$ .

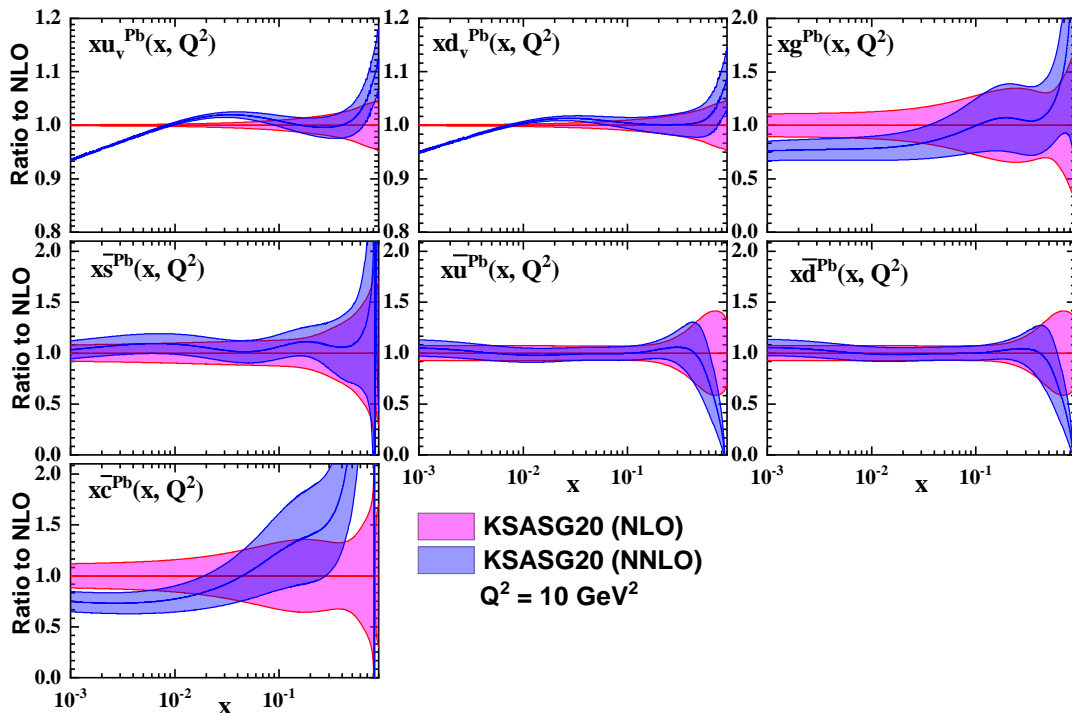


**Figure 8:** Comparison between the NLO and NNLO nuclear PDFs together with their one- $\sigma$  uncertainties. The results are shown as ratios NNLO/NLO at the scale  $Q^2 = 10 \text{ GeV}^2$  for lead.

A few remarks concerning the comparison between our NLO and NNLO analyses are in order. For both lead and iron nuclei, the valence quark,  $xu_v$  and  $xd_v$ , and strange quark  $x\bar{s}$  PDF densities at NLO and NNLO accuracy are very similar in size. The sea quark densities,  $x\bar{u}$  and  $x\bar{d}$ , are slightly different at NLO and NNLO accuracy in the region of small  $x$ ,  $x < 0.01$ . A significant difference can be found for the gluon  $xg$  and the perturbatively generated charm quark  $x\bar{c}$  density at NLO and NNLO accuracy. As can be seen from Figs. 6 and 7, the NNLO gluon and charm quark PDFs are smaller than at NLO at small values of  $x$ .

In order to give further weight to the results discussed above, we also present ratios of nuclear PDFs obtained in the NNLO fit over those of the NLO fit. This comparison is shown in Fig. 8 for lead and in Fig. 9 for gold. The results are displayed at the scale  $Q^2 = 10 \text{ GeV}^2$  and we include the one- $\sigma$  uncertainty bands for  $\Delta\chi^2 = 10$ . As can be seen, the uncertainty for the nuclear gluon density slightly decreases when going from NLO to NNLO accuracy, perhaps due to the improved overall fit quality

when higher-order QCD calculations are taken into account. However, the differences between NLO and NNLO nuclear PDFs are rather small for all other parton species. These findings are consistent with the perturbative convergence of the global  $\chi^2$  discussed in Sec. IV and listed in Tables I, II, III and IV. Concerning the fit quality of the total nuclear and neutrino datasets, the most noticeable feature is a small improvement upon inclusion of higher-order QCD corrections. The inclusion of NNLO QCD corrections affects the nuclear PDFs uncertainty and improves the description of the data as well.

### C. Comparison with other nuclear PDF sets

Before moving forward, it should be useful to illustrate qualitatively our extracted nuclear PDFs in comparison with other nuclear PDF sets. We present the comparison with the most recent nuclear PDF determinations available in the literature, namely nCTEQ15 [18], EPPS16 [5] and TUJU19 [4]. Since the nCTEQ15 and EPPS16 analyses

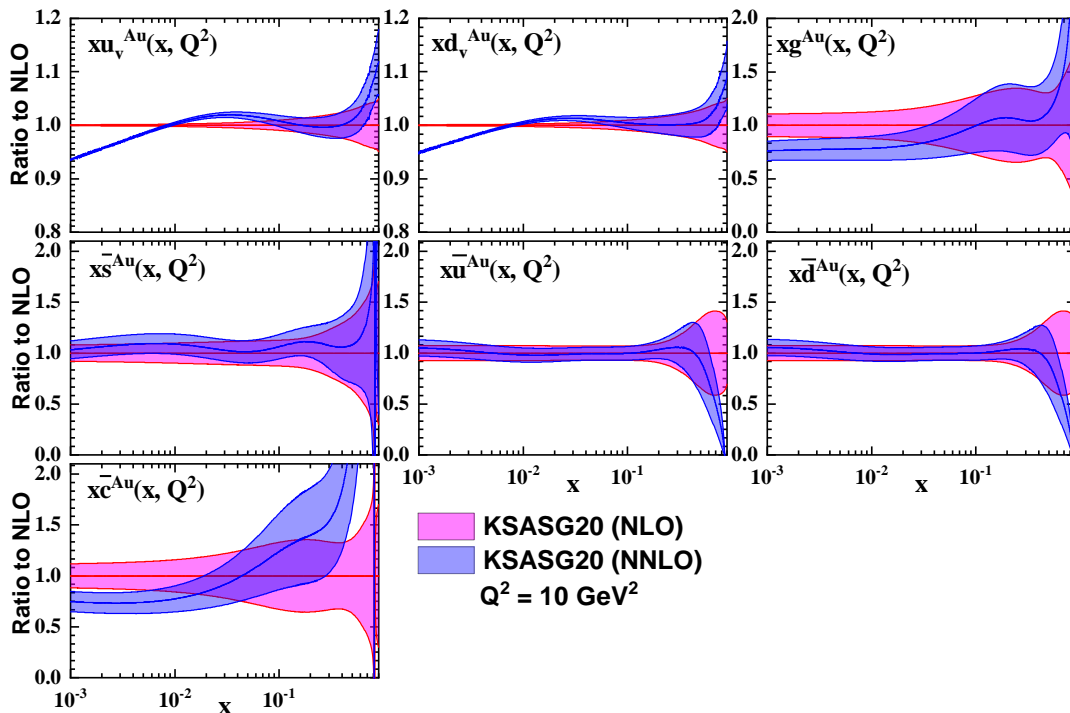


Figure 9: Same as Fig. 8, but for gold.

were performed only at NLO accuracy, we limit the comparison to this perturbative order. All the comparisons presented in this section have been generated by using the standard LHAPDF6 library [89] and the published grids.

Each of these nuclear PDF analyses is based on a set of assumptions, for example, the form of the input parameterization at the initial scale, the choice of the proton baseline PDFs, the included datasets and the kinematical cuts applied to the data, the perturbative order, and the scheme for the heavy quark contributions.

We begin with a detailed comparison with the most recent nuclear PDF determination by TUJU19. Regarding the experimental DIS data to determine the nuclear PDFs, both KSASG20 and TUJU19 are based on the same datasets with different kinematical cuts. However, in addition to the deuteron structure function  $F_2^D$  from NMC [65], we also enrich our analysis with the  $F_2^D$  data from BCDMS [66, 67] and HERMES [68], and data for the ratio  $F_2^D/F_2^p$  from NMC [69]. The TUJU19 nuclear PDF sets are based on a CTEQ proton baseline fitted within the same framework. TUJU19 also assumed flavor symmetric sea quark densities, i.e.  $\bar{u} = \bar{d} = \bar{s} = \bar{c}$ .

The uncertainties for both analyses are obtained using the Hessian method, and TUJU19 calculated the uncertainty for  $\Delta\chi^2 = 50$ .

The comparison with TUJU19 is presented in Fig. 10 at  $Q^2 = 100 \text{ GeV}^2$  for lead at NNLO accuracy. Concerning the shapes of these PDFs, a number of interesting differences between the two sets can be seen from the comparison presented in this figure. Small disagreements are found for the valence and sea-quark densities, however, the two sets still agree at the one- $\sigma$  level. A moderate difference is observed for the strange quark density below  $x < 0.1$ . A more pronounced difference in shape is observed for the gluon, charm and bottom quark PDFs, for which the KSASG20 distributions are more suppressed at medium to small values of  $x$ . The differences in shape among these three densities are more marked in the case of the gluon density. One should remember that neither of these analyses includes data which are directly sensitive to the gluon distribution. The origin of the differences between KSASG20 and TUJU19, at medium to low  $x$  for the gluon and sea-quark densities, and for medium  $x$  in the case of valence quark PDFs, is likely to be mostly

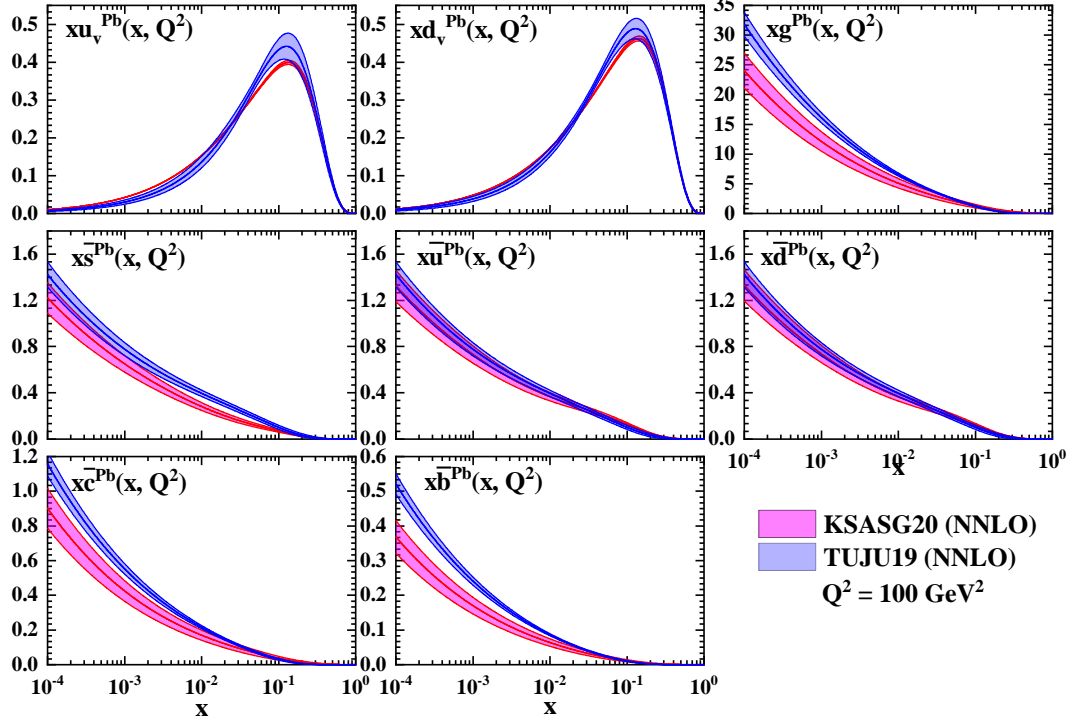


**Figure 10:** Our bound proton PDFs at the scale  $Q^2 = 100 \text{ GeV}^2$  for lead at NNLO accuracy. The most recent results from TUJU19 [4] are also shown for comparison.

due to the input parameterization and statistically more deuteron data points included in the KSASG20 analysis.

In Figs. 11 and 12, our bound proton PDFs at the scale  $Q^2 = 100 \text{ GeV}^2$  are presented for lead at NLO accuracy. The most recent NLO nuclear PDF determinations available in the literature, namely from nCTEQ15 [18], EPPS16 [5] and TUJU19 [4] are also shown for comparison. We should mention here that the nCTEQ15 analysis is based on the tolerance criterion  $\Delta\chi^2 = 35$ , while EPPS16 presented their results for  $\Delta\chi^2 = 52$ .

In the EPPS16 analysis, the bound nucleon PDFs are defined relative to the free nucleon baseline CT14 PDFs [90], as for the case of our previous study KA15 [3] which we considered the same framework and used JR PDFs [91]. The nuclear modification functions are parameterized at the input scale. The EPPS16 analysis was the first study which used data from the LHC for  $Z$  and  $W^\pm$  boson productions [26–28] and dijet production [25] in proton-lead collisions. These collider data provide further constraints for the gluon nuclear modifications and for the flavor separation. In the nCTEQ15

analysis, the nuclear PDFs are parameterized by a polynomial functional form, in which all the  $A$  dependence is encoded in the coefficients of the parameterization. nCTEQ15 assumed  $s = \bar{s}$  and the strange quark density is related to  $\bar{u} + \bar{d}$  by an additional  $A$ -dependent factor,  $s = \bar{s} = (\kappa(A)/2)(\bar{u} + \bar{d})$ . The TUJU19 analysis considered flavor symmetry for the sea quark densities,  $\bar{u} = \bar{d} = s = \bar{s}$ , while in EPPS16 and KSASG20 only  $s = \bar{s}$  was used as a constraint.

After presenting the main properties of these recent nuclear PDFs, we compare their results at NLO accuracy. As can be seen from Fig. 11, for the  $xu_v$  and  $xd_v$  densities, the KSASG20 results are in agreement in size with TUJU19, nCTEQ15 and EPPS16, and well within their uncertainties, despite differences in the dataset and parametrization, etc. For the valence quark densities we find that both KSASG20  $xu_v$  and  $xd_v$  slightly tend to stay below all other results at medium values of  $x$ ;  $x \sim 0.1$ . Moderate differences for the gluon density and significant differences for the sea-quark densities are observed. For both cases, EPPS16 exhibits relatively wider error bands

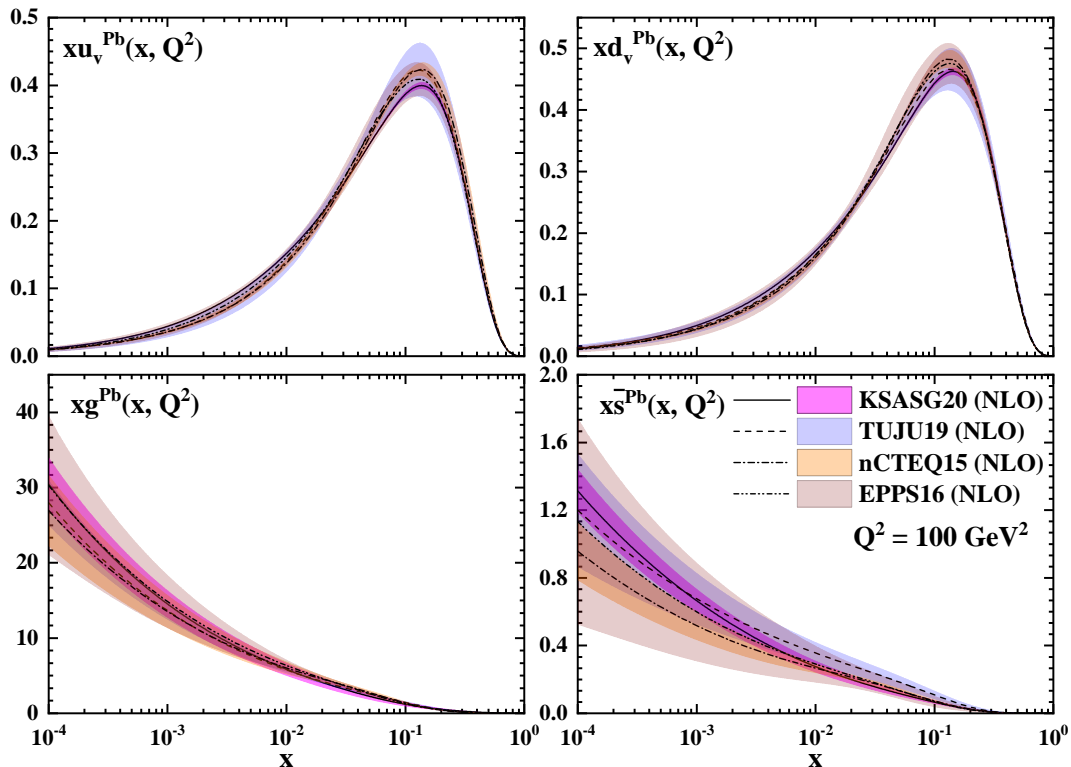


**Figure 11:** Our bound proton PDFs at the scale  $Q^2 = 100 \text{ GeV}^2$  for lead at NLO accuracy. The most recent results from nCTEQ15 [18], EPPS16 [5] and TUJU19 [4] are shown for comparison. The comparison is presented for the distribution functions  $xf_i(x, Q^2 = 100 \text{ GeV}^2)$  per parton flavor  $u_v, d_v, g$  and  $\bar{s}$ .

compared with other analyses. The gluon distributions from nCTEQ15 and EPPS16 fall below the one of KSASG20.

In Fig. 12 we show a comparison for the sea-quark distributions (upper row) and the charm and the bottom distributions (lower row). The latter two are perturbatively generated. We find agreement between the results of KSASG20 and TUJU19 both for the central values and for the uncertainties in the whole range of  $x$ . Moderate differences between KSASG20, nCTEQ15 and EPPS16 can be seen for all densities displayed in Fig. 12. The resulting uncertainties for KSASG20 are somewhat smaller than the other two. We should stress again that all results presented here are based on the choice  $\Delta\chi^2 = 10$  for the tolerance. Choosing the larger tolerance value  $\Delta\chi^2 = 50$ , as preferred by other groups, the error bands of our nuclear PDFs would increase by a factor of  $\sim 2$ .

#### D. Fit quality and comparison of data and theory

In Tables I, II, III, IV and V presented above in section III we have shown the values of  $\chi^2$  per data point for each individual dataset, both for the NLO and the NNLO fits. In total, we find for the KSASG20 fit at NLO,  $\chi^2 = 5202.53$  with 4525 data points. With 9 free parameters this leads to a  $\chi^2/\text{d.o.f} = 1.25$  which indicates a relatively good fit. At NNLO, the KSASG20 fit leads to  $\chi^2/\text{d.o.f} = 1.22$ . This is only a moderate improvement upon inclusion of the higher-order QCD corrections.

While most datasets for nuclear and neutrino DIS experiments satisfy the goodness of fit criterion, there are some experiments which stand out as having a poor fit. We also notice that for some datasets,  $\chi^2$  is poor even at NNLO accuracy. In addition, for some individual datasets  $\chi^2$  increases as higher-order QCD corrections are included. These results were already observed in previous analyses by TUJU19 [4] and nNNPDF1.0 [1].

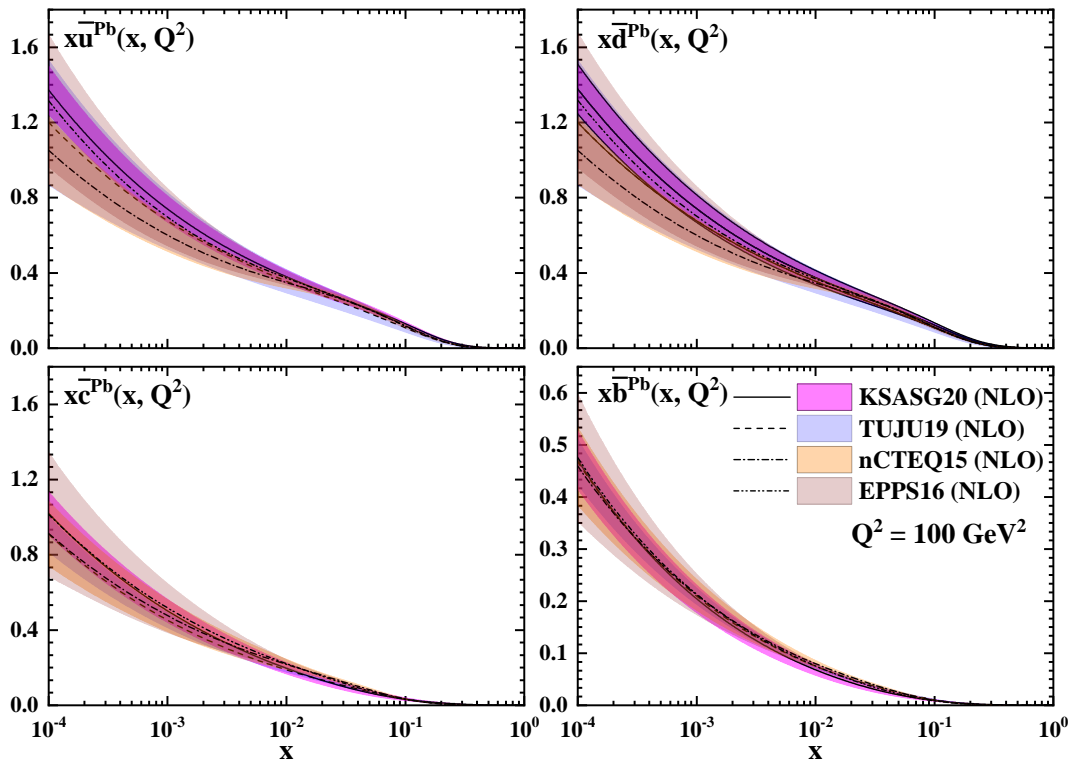


**Figure 12:** Same as Fig. 11, but for the distribution functions  $x f_i(x, Q^2 = 100 \text{ GeV}^2)$  per parton flavor  $\bar{u}$ ,  $\bar{d}$ ,  $\bar{c}$ , and  $\bar{b}$ .

As one can see from Table IV, with the exception of  $\nu\text{Pb}$  data from CHORUS, for all other (anti)neutrino-nucleus DIS data the inclusion of higher-order QCD corrections leads to a better fit quality.

In order to give further weight to our discussion on the fit quality and obtained  $\chi^2$ , in the following we present several comparisons of the datasets used in this study to the corresponding NNLO theoretical predictions obtained using the KSASG20 NNLO nuclear PDFs. In Fig. 13 such a comparison is displayed for the nuclear DIS data for the ratio  $F_2^A(x, Q^2)/F_2^C(x, Q^2)$  as a function of  $x$  at  $Q^2 = 5 \text{ GeV}^2$ . Our NNLO theory predictions have been calculated at the  $Q^2$  values of the corresponding data point. In Fig. 14 we also compare our NNLO theory predictions for  $F_2^A(x, Q^2)/F_2^D(x, Q^2)$  and  $F_2^A(x, Q^2)/F_2^{Li}(x, Q^2)$  as a function of  $x$  with some selected nuclear DIS data at  $Q^2 = 5 \text{ GeV}^2$ . The data shown in these plots are measured by the NMC and E139 Collaborations. The bands show the 68% uncertainty estimates with  $\Delta\chi^2 = 10$  obtained using the Hessian method. The comparisons presented in these plots

demonstrate that the agreement between our NNLO theoretical predictions and the nuclear DIS experimental measurements varies between different data for different nuclei. Apart from a few data points in the small- $x$  region, the agreement with most of the data published by the NMC and E139 Collaborations is excellent.

A promising avenue for significant improvements in the determination of nuclear PDFs is to include data for neutrino(antineutrino) induced DIS off iron and lead targets available from neutrino experiments. The neutrino(antineutrino) data receive their importance in discriminating power between the nuclear modifications for the quark and antiquark densities. A detailed comparison with the CHORUS data on neutrino(antineutrino) lead collisions [71] and the CDHSW data on neutrino(antineutrino) iron collisions [70] are shown in Figs. 15 and 16, respectively. The results are shown as a function of  $Q^2$  for some selected bins of  $x$  and  $y$ . The incident beam of neutrino(antineutrino) energies are not high enough to reach small values of  $x$ , and here we consider the  $x = 0.125$  to  $x = 0.65$ . The selected

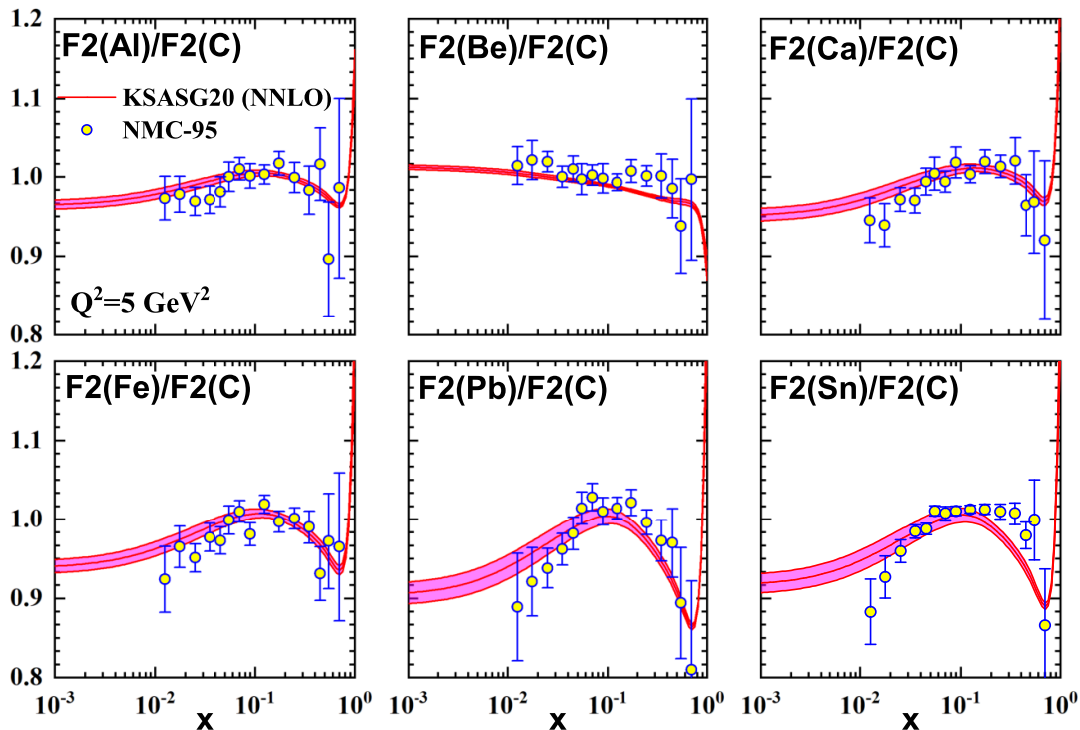


**Figure 13:** Comparison of our NNLO theory predictions for the ratio  $F_2^A(x, Q^2)/F_2^C(x, Q^2)$  as a function of  $x$  with some selected nuclear DIS data. Our NNLO theory predictions have been calculated at the  $Q^2$  values of the corresponding data point. The bands show the 68% uncertainty estimate with  $\Delta\chi^2 = 10$  obtained using the Hessian method.

data correspond to the bins of  $y = 0.3$  and  $y = 0.5$ . Interestingly, very good agreement is achieved for the neutrino(antineutrino)-nucleus data presented in these plots for the whole region of  $x$  and  $Q^2$ .

## VI. SUMMARY AND CONCLUSIONS

In summary, in this work, we have introduced a new set of nuclear PDFs at NLO and NNLO accuracy in pQCD. Flavor dependent nuclear PDFs are obtained from the most up-to-date neutral-current nuclear DIS and charged-current neutrino DIS datasets with several nuclear targets, which are sensitive to the valence quark density and allow a separation of up- and down-type quarks. Heavy quark mass effects are included in the FONLL general-mass variable-flavor-number scheme (GM-VFNS) for charm and bottom quarks. The determination of nuclear PDFs includes error estimates obtained within the Hessian method with the tolerance criterion

of  $\Delta\chi^2 = 10$ . The effects arising from the inclusion of higher-order QCD corrections are investigated. We found a small difference between the NLO and NNLO QCD fits, both for the shape and size of the uncertainty bands. We find that for the gluon nuclear PDF, our NNLO fit leads to a slight decrease in the uncertainties.

In contrast to the other recent analyses, such as nNNPDF2.0 [1] and nNNPDF2.1 [2] which use Monte Carlo techniques based on the NNPDF framework, and TUJU19 [4] which is based on the CTEQ framework, we parameterize the nuclear PDFs considering well-established nuclear correction factors. To this end, a modern set of parton distribution functions for free protons, namely CT18, are considered as reference. Our results are consistent, within uncertainties, with the previous determinations of nuclear PDFs available in the literature, in particular for nCTEQ15 [18], EPPS16 [5] and TUJU19, which are based on different datasets and assumptions. However, we found a number of differences which only occur in regions without any constraints from

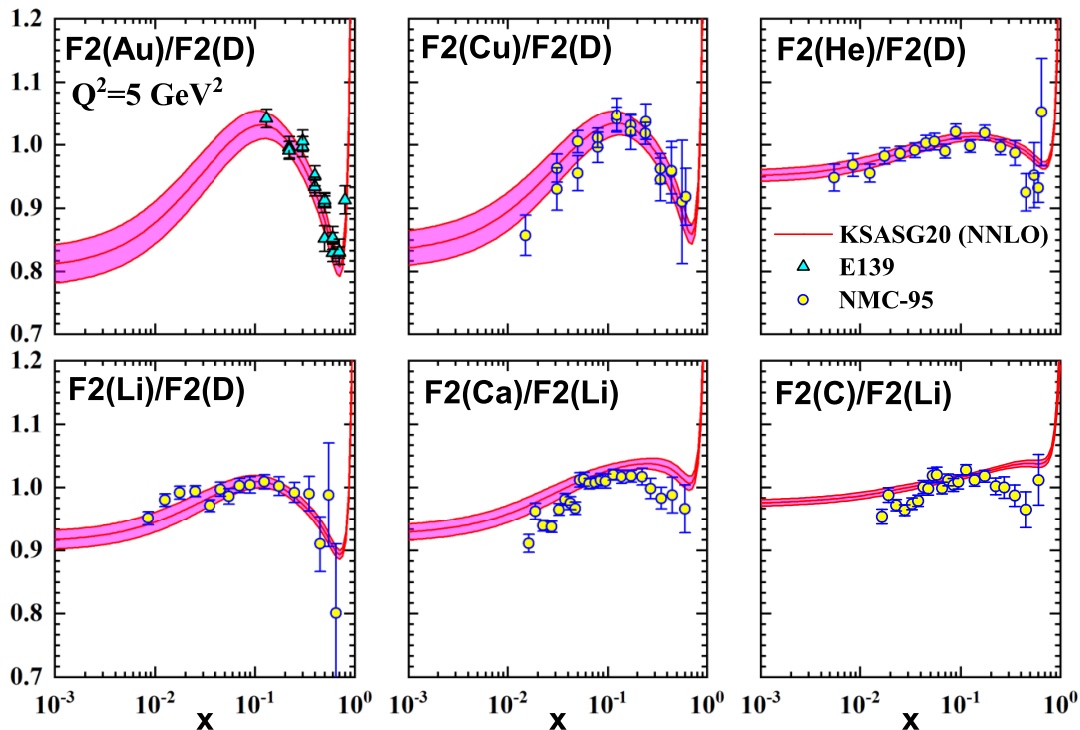


**Figure 14:** Comparison of our NNLO theory predictions for the ratios  $F_2^A(x, Q^2)/F_2^D(x, Q^2)$  and  $F_2^A(x, Q^2)/F_2^{Li}(x, Q^2)$  as a function of  $x$  with some selected nuclear DIS data.

data. These differences can be attributed to different assumptions such as input parametrization of the nuclear effects.

While the input nuclear and neutrino DIS datasets used in this study allowed us to determine the nuclear quark and anti-quark densities, the nuclear gluon PDF is only loosely constrained by these data. To resolve this limitation, we plan to include additional datasets, especially from present and future measurements of proton-lead and lead-lead collisions at the CERN-LHC, which are expected to provide direct information on the nuclear gluon modifications and more stringent flavor-dependence constraints. Further in the future, the electron-ion collider (EIC) [92], the Large Hadron-Electron Collider (LHeC) [93] or Future Circular Collider (FCC) [94, 95] could provide precise data for nuclear PDF analyses. In terms of future work, it would be very interesting to repeat the analysis described here using additional observables from hadron colliders such as the LHC.

The NLO and NNLO nuclear PDF sets presented in

this work are available in the LHAPDF format [89] for all relevant nuclei from  $A = 1$  to  $A = 208$  and can be obtained from the authors upon request.

## ACKNOWLEDGMENTS

The authors are thankful to Valerio Bertone, Hamed Abdolmaleki and Muhammad Goharipour for many helpful discussions and comments. The authors thank the School of Particles and Accelerators, Institute for Research in Fundamental Sciences (IPM) for financial support of this project. Hamzeh Khanpour also is grateful to the University of Science and Technology of Mazandaran for financial support of this project.

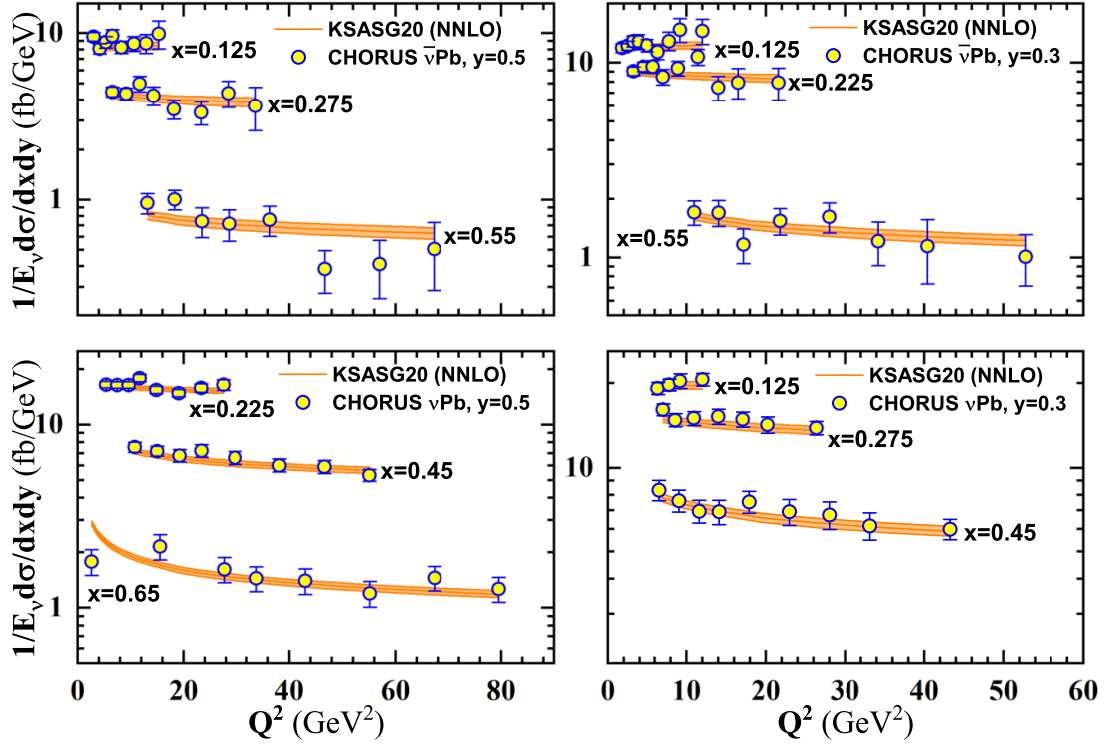


**Figure 15:** The neutrino(antineutrino) lead DIS data from the CHORUS measurements [71], compared with the KSASG20 NNLO theory predictions. The bands show the 68% uncertainty estimates with  $\Delta\chi^2 = 10$  obtained using the Hessian method.

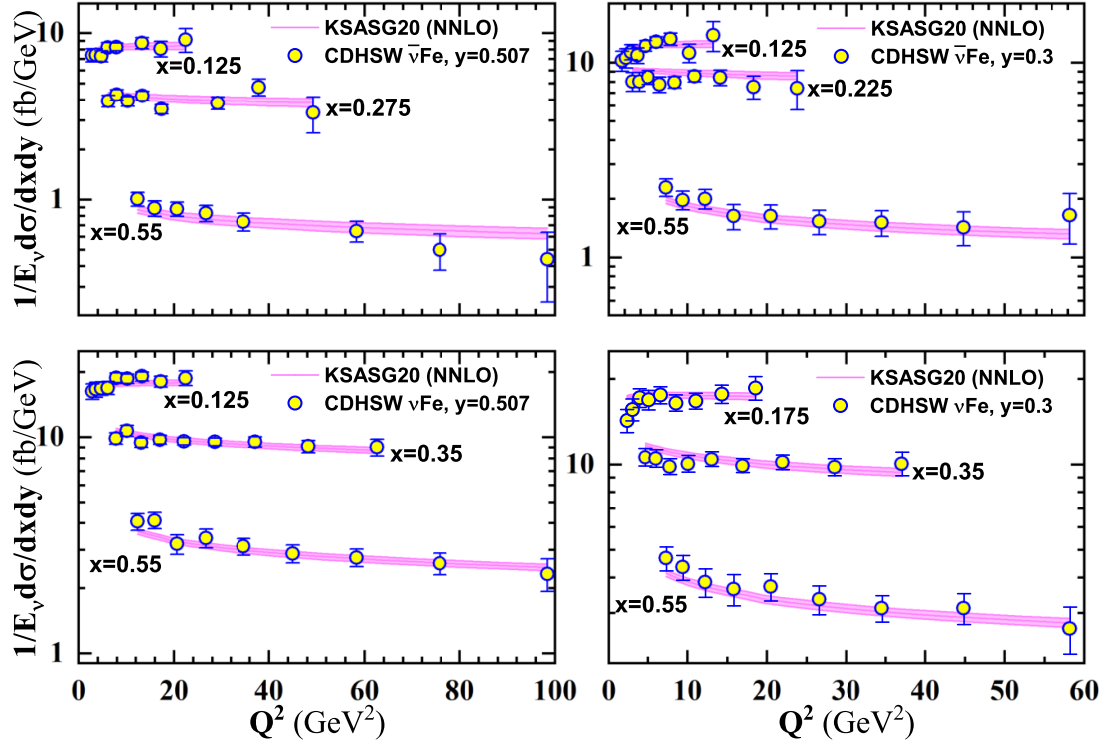


Figure 16: Same as Fig. 15, but for the neutrino(antineutrino) iron DIS data from the CDHSW measurements [70].

- [1] R. Abdul Khalek *et al.* [NNPDF Collaboration], “Nuclear parton distributions from lepton-nucleus scattering and the impact of an electron-ion collider,” *Eur. Phys. J. C* **79**, no. 6, 471 (2019), [arXiv:1904.00018 [hep-ph]].
- [2] R. Abdul Khalek, J. J. Ethier, J. Rojo and G. van Weelden, “nNNPDF2.0: Quark Flavor Separation in Nuclei from LHC Data,” arXiv:2006.14629 [hep-ph].
- [3] H. Khanpour and S. Atashbar Tehrani, “Global Analysis of Nuclear Parton Distribution Functions and Their Uncertainties at Next-to-Next-to-Leading Order,” *Phys. Rev. D* **93**, no. 1, 014026 (2016), [arXiv:1601.00939 [hep-ph]].
- [4] M. Walt, I. Helenius and W. Vogelsang, “Open-source QCD analysis of nuclear parton distribution functions at NLO and NNLO,” *Phys. Rev. D* **100**, no. 9, 096015 (2019), [arXiv:1908.03355 [hep-ph]].
- [5] K. J. Eskola, P. Paakkinen, H. Paukkunen and C. A. Salgado, “EPPS16: Nuclear parton distributions with LHC data,” *Eur. Phys. J. C* **77**, no. 3, 163 (2017), [arXiv:1612.05741 [hep-ph]].
- [6] H. Paukkunen and P. Zurita, “Can we fit nuclear PDFs with the high-x CLAS data?,” *Eur. Phys. J. C* **80**, no. 5, 381 (2020) [arXiv:2003.02195 [hep-ph]].
- [7] P. Ru, S. A. Kulagin, R. Petti and B. W. Zhang, “Study of  $W^\pm$  and  $Z$  boson production in proton-lead collisions at the LHC with Kulagin-Petti nuclear parton distributions,” *Phys. Rev. D* **94**, no. 11, 113013 (2016) [arXiv:1608.06835 [nucl-th]].
- [8] R. Wang, X. Chen and Q. Fu, “Global study of nuclear modifications on parton distribution functions,” *Nucl. Phys. B* **920**, 1 (2017) [arXiv:1611.03670 [hep-ph]].
- [9] A. Kusina *et al.*, “Vector boson production in pPb and PbPb collisions at the LHC and its impact on nCTEQ15 PDFs,” *Eur. Phys. J. C* **77**, no. 7, 488 (2017) [arXiv:1610.02925 [nucl-th]].
- [10] S. Atashbar Tehrani, “Nuclear parton densities and their uncertainties at the next-to-leading order,” *Phys. Rev. C* **86**, 064301 (2012).
- [11] S. A. Kulagin and R. Petti, “Nuclear parton distributions and the Drell-Yan process,” *Phys. Rev. C* **90**, no. 4, 045204 (2014) [arXiv:1405.2529 [hep-ph]].
- [12] D. de Florian, R. Sassot, P. Zurita and M. Stratmann, “Global Analysis of Nuclear Parton Distributions,” *Phys. Rev. D* **85**, 074028 (2012) [arXiv:1112.6324 [hep-ph]].
- [13] K. J. Eskola, H. Paukkunen and C. A. Salgado, “An Improved global analysis of nuclear parton distribution functions including RHIC data,” *JHEP* **0807**, 102 (2008) [arXiv:0802.0139 [hep-ph]].
- [14] K. Kovarik, I. Schienbein, F. I. Olness, J. Y. Yu, C. Keppel, J. G. Morfin, J. F. Owens and T. Stavreva, “Nuclear Corrections in Neutrino-Nucleus DIS and Their Compatibility with Global NPFD Analyses,” *Phys. Rev. Lett.* **106**, 122301 (2011) [arXiv:1012.0286 [hep-ph]].
- [15] K. J. Eskola, H. Paukkunen and C. A. Salgado, “EPS09: A New Generation of NLO and LO Nuclear Parton Distribution Functions,” *JHEP* **0904**, 065 (2009) [arXiv:0902.4154 [hep-ph]].
- [16] M. Hirai, S. Kumano and M. Miyama, “Determination of nuclear parton distributions,” *Phys. Rev. D* **64**, 034003 (2001) [hep-ph/0103208].
- [17] M. Hirai, S. Kumano and T.-H. Nagai, “Determination of nuclear parton distribution functions and their uncertainties in next-to-leading order,” *Phys. Rev. C* **76**, 065207 (2007) [arXiv:0709.3038 [hep-ph]].
- [18] K. Kovarik *et al.*, “nCTEQ15 - Global analysis of nuclear parton distributions with uncertainties in the CTEQ framework,” *Phys. Rev. D* **93**, no. 8, 085037 (2016) [arXiv:1509.00792 [hep-ph]].
- [19] D. de Florian, R. Sassot, M. Stratmann and P. Zurita, “Global Analysis of Nuclear PDFs,” arXiv:1204.3797 [hep-ph].
- [20] Y. L. Dokshitzer, “Calculation of the Structure Functions for Deep Inelastic Scattering and  $e^+e^-$  Annihilation by Perturbation Theory in Quantum Chromodynamics,” *Sov. Phys. JETP* **46**, 641 (1977) [*Zh. Eksp. Teor. Fiz.* **73**, 1216 (1977)].
- [21] V. N. Gribov and L. N. Lipatov, “Deep inelastic  $e p$  scattering in perturbation theory,” *Sov. J. Nucl. Phys.* **15**, 438 (1972) [*Yad. Fiz.* **15**, 781 (1972)].
- [22] L. N. Lipatov, “The parton model and perturbation theory,” *Sov. J. Nucl. Phys.* **20**, 94 (1975) [*Yad. Fiz.* **20**, 181 (1974)].
- [23] G. Altarelli and G. Parisi, “Asymptotic Freedom in Parton Language,” *Nucl. Phys. B* **126**, 298 (1977).
- [24] S. Alekhin *et al.*, “HERAFitter,” *Eur. Phys. J. C* **75**, no. 7, 304 (2015) [arXiv:1410.4412 [hep-ph]].
- [25] S. Chatrchyan *et al.* [CMS Collaboration], “Studies of dijet transverse momentum balance and pseudorapidity distributions in pPb collisions at  $\sqrt{s_{NN}} = 5.02$  TeV,” *Eur. Phys. J. C* **74**, no. 7, 2951 (2014), [arXiv:1401.4433 [nucl-ex]].
- [26] V. Khachatryan *et al.* [CMS Collaboration], “Study of  $W$  boson production in pPb collisions at  $\sqrt{s_{NN}} = 5.02$  TeV,” *Phys. Lett. B* **750**, 565 (2015), [arXiv:1503.05825 [nucl-ex]].
- [27] V. Khachatryan *et al.* [CMS Collaboration], “Study of  $Z$  boson production in pPb collisions at  $\sqrt{s_{NN}} = 5.02$  TeV,” *Phys. Lett. B* **759**, 36 (2016), [arXiv:1512.06461 [hep-ex]].
- [28] G. Aad *et al.* [ATLAS Collaboration], “ $Z$  boson production in  $p$ +Pb collisions at  $\sqrt{s_{NN}} = 5.02$  TeV measured with the ATLAS detector,” *Phys. Rev. C* **92**, no. 4, 044915 (2015), [arXiv:1507.06232 [hep-ex]].
- [29] A. M. Sirunyan *et al.* [CMS Collaboration], “Observation of nuclear modifications in  $W^\pm$  boson production in pPb collisions at  $\sqrt{s_{NN}} = 8.16$  TeV,” *Phys. Lett. B* **800**, 135048 (2020) [arXiv:1905.01486 [hep-ex]].
- [30] V. Bertone, S. Carrazza and J. Rojo, “APFEL: A PDF Evolution Library with QED corrections,” *Comput. Phys. Commun.* **185**, 1647 (2014) [arXiv:1310.1394 [hep-ph]].
- [31] T. J. Hou *et al.*, “Progress in the CTEQ-TEA NNLO global QCD analysis,” arXiv:1908.11394 [hep-ph].
- [32] N. Armesto, H. Paukkunen, J. M. Penín, C. A. Salgado and P. Zurita, “An analysis of the impact of LHC Run I proton-lead data on nuclear parton densities,” *Eur. Phys. J. C* **76**, no.4, 218 (2016), [arXiv:1512.01528 [hep-ph]].
- [33] K. J. Eskola, P. Paakkinen and H. Paukkunen, “Non-quadratic improved Hessian PDF reweighting and application to CMS dijet measurements at 5.02 TeV,” *Eur. Phys. J. C* **79**, no.6, 511 (2019), [arXiv:1903.09832 [hep-ph]].

- ph]].
- [34] H. Paukkunen and C. A. Salgado, “Agreement of Neutrino Deep Inelastic Scattering Data with Global Fits of Parton Distributions,” *Phys. Rev. Lett.* **110**, no.21, (2013), [arXiv:1302.2001 [hep-ph]].
- [35] H. Paukkunen and P. Zurita, “PDF reweighting in the Hessian matrix approach,” *JHEP* **12**, 100 (2014). [arXiv:1402.6623 [hep-ph]].
- [36] K. J. Eskola, I. Helenius, P. Paakkinen and H. Paukkunen, “A QCD analysis of LHCb D-meson data in p+Pb collisions,” *JHEP* **05**, 037 (2020), [arXiv:1906.02512 [hep-ph]].
- [37] R. Aaij *et al.* [LHCb Collaboration], “Study of prompt  $D^0$  meson production in pPb collisions at  $\sqrt{s_{NN}} = 5$  TeV,” *JHEP* **1710**, 090 (2017), [arXiv:1707.02750 [hep-ex]].
- [38] H. Paukkunen, “Nuclear PDFs in the beginning of the LHC era,” *Nucl. Phys. A* **926**, 24 (2014), [arXiv:1401.2345 [hep-ph]].
- [39] K. Rith, “Present Status of the EMC effect,” *Subnucl. Ser.* **51**, 431 (2015) [arXiv:1402.5000 [hep-ex]].
- [40] K. J. Eskola, “Global analysis of nuclear PDFs - latest developments,” *Nucl. Phys. A* **910-911**, 163 (2013) [arXiv:1209.1546 [hep-ph]].
- [41] I. Sick and D. Day, “The EMC effect of nuclear matter,” *Phys. Lett. B* **274**, 16 (1992).
- [42] A. Accardi *et al.*, “A Critical Appraisal and Evaluation of Modern PDFs,” *Eur. Phys. J. C* **76**, no. 8, 471 (2016) [arXiv:1603.08906 [hep-ph]].
- [43] A. D. Martin, W. J. Stirling, R. S. Thorne and G. Watt, “Parton distributions for the LHC,” *Eur. Phys. J. C* **63**, 189-285 (2009) [arXiv:0901.0002 [hep-ph]].
- [44] S. Forte, E. Laenen, P. Nason and J. Rojo, “Heavy quarks in deep-inelastic scattering,” *Nucl. Phys. B* **834**, 116 (2010) [arXiv:1001.2312 [hep-ph]].
- [45] M. Cacciari, M. Greco and P. Nason, “The P(T) spectrum in heavy flavor hadroproduction,” *JHEP* **9805**, 007 (1998) [hep-ph/9803400].
- [46] V. Bertone, “Higher Order and Heavy Quark Mass Effects in the Determination of Parton Distribution Functions,” <http://nnpdf.mi.infn.it/wp-content/uploads/2017/10/VBertone-thesis.pdf>.
- [47] M. Tanabashi *et al.* [Particle Data Group], “Review of Particle Physics,” *Phys. Rev. D* **98**, no. 3, 030001 (2018).
- [48] J. Ashman *et al.* [European Muon Collaboration], “A Measurement of the ratio of the nucleon structure function in copper and deuterium,” *Z. Phys. C* **57**, 211 (1993).
- [49] P. Amaudruz *et al.* [New Muon Collaboration], “A Reevaluation of the nuclear structure function ratios for D, He, Li-6, C and Ca,” *Nucl. Phys. B* **441**, 3 (1995) [hep-ph/9503291].
- [50] J. Ashman *et al.* [European Muon Collaboration], “Measurement of the Ratios of Deep Inelastic Muon - Nucleus Cross-Sections on Various Nuclei Compared to Deuterium,” *Phys. Lett. B* **202**, 603 (1988).
- [51] M. Arneodo *et al.* [New Muon Collaboration], “The Structure Function ratios  $F2(\text{li}) / F2(\text{D})$  and  $F2(\text{C}) / F2(\text{D})$  at small  $x$ ,” *Nucl. Phys. B* **441**, 12 (1995) [hep-ex/9504002].
- [52] G. Bari *et al.* [BCDMS Collaboration], “A Measurement of Nuclear Effects in Deep Inelastic Muon Scattering on Deuterium, Nitrogen and Iron Targets,” *Phys. Lett.* **163B**, 282 (1985).
- [53] M. Arneodo *et al.* [New Muon Collaboration], “The A dependence of the nuclear structure function ratios,” *Nucl. Phys. B* **481**, 3 (1996).
- [54] A. C. Benvenuti *et al.* [BCDMS Collaboration], “Nuclear Effects in Deep Inelastic Muon Scattering on Deuterium and Iron Targets,” *Phys. Lett. B* **189**, 483 (1987).
- [55] M. Arneodo *et al.* [New Muon Collaboration], “The  $Q^{*2}$  dependence of the structure function ratio  $F2 \text{ Sn} / F2 \text{ C}$  and the difference  $R \text{ Sn} - R \text{ C}$  in deep inelastic muon scattering,” *Nucl. Phys. B* **481**, 23 (1996).
- [56] J. Gomez *et al.*, “Measurement of the A-dependence of deep inelastic electron scattering,” *Phys. Rev. D* **49**, 4348 (1994).
- [57] A. Bodek *et al.*, “A Comparison of the Deep Inelastic Structure Functions of Deuterium and Aluminum Nuclei,” *Phys. Rev. Lett.* **51**, 534 (1983).
- [58] A. Bodek *et al.*, “Electron Scattering from Nuclear Targets and Quark Distributions in Nuclei,” *Phys. Rev. Lett.* **50**, 1431 (1983).
- [59] M. Arneodo *et al.* [European Muon Collaboration], “Measurements of the nucleon structure function in the range  $0.002 - \text{GeV}^2 < x < 0.17 - \text{GeV}^2$  and  $0.2 - \text{GeV}^2 < q^2 < 8 - \text{GeV}^2$  in deuterium, carbon and calcium,” *Nucl. Phys. B* **333**, 1 (1990).
- [60] S. Dasu *et al.*, “Measurement of the Difference in  $R = \sigma^{-1} / \sigma^{-t}$  and  $\sigma(a) / \sigma(D)$  in Deep Inelastic  $eD$ ,  $e \text{ Fe}$  and  $e \text{ Au}$  Scattering,” *Phys. Rev. Lett.* **60**, 2591 (1988).
- [61] K. Ackerstaff *et al.* [HERMES Collaboration], “Nuclear effects on  $R = \sigma_L / \sigma_T$  in deep inelastic scattering,” *Phys. Lett. B* **475**, 386 (2000) Erratum: [*Phys. Lett. B* **567**, 339 (2003)] [hep-ex/9910071, hep-ex/0210067].
- [62] J. Seely *et al.*, “New measurements of the EMC effect in very light nuclei,” *Phys. Rev. Lett.* **103**, 202301 (2009) [arXiv:0904.4448 [nucl-ex]].
- [63] M. R. Adams *et al.* [E665 Collaboration], “Saturation of shadowing at very low  $x_{\text{BJ}}$ ,” *Phys. Rev. Lett.* **68**, 3266 (1992).
- [64] M. R. Adams *et al.* [E665 Collaboration], “Shadowing in inelastic scattering of muons on carbon, calcium and lead at low  $x(\text{Bj})$ ,” *Z. Phys. C* **67**, 403 (1995) [hep-ex/9505006].
- [65] M. Arneodo *et al.* [New Muon Collaboration], “Measurement of the proton and deuteron structure functions,  $F2(\text{p})$  and  $F2(\text{d})$ , and of the ratio  $\sigma\text{-L} / \sigma\text{-T}$ ,” *Nucl. Phys. B* **483**, 3 (1997), [hep-ph/9610231].
- [66] M. R. Adams *et al.* [E665 Collaboration], “Proton and deuteron structure functions in muon scattering at 470-GeV,” *Phys. Rev. D* **54**, 3006 (1996).
- [67] A. C. Benvenuti *et al.* [BCDMS Collaboration], “A High Statistics Measurement of the Deuteron Structure Functions  $F2(X, Q^2)$  and  $R$  From Deep Inelastic Muon Scattering at High  $Q^2$ ,” *Phys. Lett. B* **237**, 592 (1990).
- [68] A. Airapetian *et al.* [HERMES Collaboration], “Inclusive Measurements of Inelastic Electron and Positron Scattering from Unpolarized Hydrogen and Deuterium Targets,” *JHEP* **1105**, 126 (2011), [arXiv:1103.5704 [hep-ex]].
- [69] M. Arneodo *et al.* [New Muon Collaboration], “Accurate measurement of  $F2(\text{d}) / F2(\text{p})$  and  $R^{*d} - R^{*p}$ ,” *Nucl. Phys. B* **487**, 3 (1997), [hep-ex/9611022].
- [70] J. P. Berge *et al.*, “A Measurement of Differential Cross-Sections and Nucleon Structure Functions in Charged Current Neutrino Interactions on Iron,” *Z. Phys. C* **49**, 187 (1991).
- [71] G. Onengut *et al.* [CHORUS Collaboration], “Measurement of nucleon structure functions in neutrino scattering,” *Phys. Lett. B* **632**, 65 (2006).

- [72] M. Tzanov *et al.* [NuTeV Collaboration], “Precise measurement of neutrino and anti-neutrino differential cross sections,” *Phys. Rev. D* **74**, 012008 (2006), [hep-ex/0509010].
- [73] D. MacFarlane *et al.*, “Nucleon Structure Functions from High-Energy Neutrino Interactions with Iron and QCD Results,” *Z. Phys. C* **26**, 1 (1984).
- [74] I. Schienbein, J. Y. Yu, C. Keppel, J. G. Morfin, F. Olness and J. F. Owens, “Nuclear parton distribution functions from neutrino deep inelastic scattering,” *Phys. Rev. D* **77**, 054013 (2008), [arXiv:0710.4897 [hep-ph]].
- [75] I. Schienbein, J. Y. Yu, K. Kovarik, C. Keppel, J. G. Morfin, F. Olness and J. F. Owens, “PDF Nuclear Corrections for Charged and Neutral Current Processes,” *Phys. Rev. D* **80**, 094004 (2009), [arXiv:0907.2357 [hep-ph]].
- [76] S. M. Moosavi Nejad, H. Khanpour, S. Atashbar Tehrani and M. Mahdavi, “QCD analysis of nucleon structure functions in deep-inelastic neutrino-nucleon scattering: Laplace transform and Jacobi polynomials approach,” *Phys. Rev. C* **94**, no. 4, 045201 (2016), [arXiv:1609.05310 [hep-ph]].
- [77] H. Paukkunen and C. A. Salgado, “Compatibility of neutrino DIS data and global analyses of parton distribution functions,” *JHEP* **1007**, 032 (2010), [arXiv:1004.3140 [hep-ph]].
- [78] J. Blumlein, H. Bottcher and A. Guffanti, “Non-singlet QCD analysis of deep inelastic world data at  $O(\alpha(s)^3)$ ,” *Nucl. Phys. B* **774**, 182 (2007), [hep-ph/0607200].
- [79] D. Stump, J. Pumplin, R. Brock, D. Casey, J. Huston, J. Kalk, H. L. Lai and W. K. Tung, “Uncertainties of predictions from parton distribution functions. 1. The Lagrange multiplier method,” *Phys. Rev. D* **65**, 014012 (2001), [hep-ph/0101051].
- [80] F. James and M. Roos, “Minuit: A System for Function Minimization and Analysis of the Parameter Errors and Correlations,” *Comput. Phys. Commun.* **10**, 343 (1975); F. James, “MINUIT Function Minimization and Error Analysis: Reference Manual Version 94.1,” CERN-D-506, CERN-D506.
- [81] J. Pumplin, D. R. Stump and W. K. Tung, “Multivariate fitting and the error matrix in global analysis of data,” *Phys. Rev. D* **65**, 014011 (2001) [hep-ph/0008191].
- [82] J. Pumplin, D. Stump, R. Brock, D. Casey, J. Huston, J. Kalk, H. L. Lai and W. K. Tung, “Uncertainties of predictions from parton distribution functions. 2. The Hessian method,” *Phys. Rev. D* **65**, 014013 (2001) [hep-ph/0101032].
- [83] N. P. Hartland, F. Maltoni, E. R. Nocera, J. Rojo, E. Slade, E. Vryonidou and C. Zhang, “A Monte Carlo global analysis of the Standard Model Effective Field Theory: the top quark sector,” *JHEP* **1904**, 100 (2019), [arXiv:1901.05965 [hep-ph]].
- [84] M. A. Vasilev *et al.* [NuSea Collaboration], “Parton energy loss limits and shadowing in Drell-Yan dimuon production,” *Phys. Rev. Lett.* **83**, 2304 (1999) [hep-ex/9906010].
- [85] D. M. Alde *et al.*, “Nuclear dependence of dimuon production at 800-GeV. FNAL-772 experiment,” *Phys. Rev. Lett.* **64**, 2479 (1990).
- [86] S. S. Adler *et al.* [PHENIX Collaboration], “Centrality dependence of pi0 and eta production at large transverse momentum in s(NN)<sup>1/2</sup> = 200-GeV d+Au collisions,” *Phys. Rev. Lett.* **98**, 172302 (2007) [nucl-ex/0610036].
- [87] B. I. Abelev *et al.* [STAR Collaboration], “Inclusive  $\pi^0$ ,  $\eta$ , and direct photon production at high transverse momentum in  $p + p$  and  $d + Au$  collisions at  $\sqrt{s_{NN}} = 200$  GeV,” *Phys. Rev. C* **81**, 064904 (2010) [arXiv:0912.3838 [hep-ex]].
- [88] J. Adams *et al.* [STAR Collaboration], “Identified hadron spectra at large transverse momentum in  $p + p$  and  $d + Au$  collisions at s(NN)<sup>1/2</sup> = 200-GeV,” *Phys. Lett. B* **637**, 161 (2006) [nucl-ex/0601033].
- [89] A. Buckley, J. Ferrando, S. Lloyd, K. Nordström, B. Page, M. Rüfenacht, M. Schönherr and G. Watt, “LHAPDF6: parton density access in the LHC precision era,” *Eur. Phys. J. C* **75**, 132 (2015) [arXiv:1412.7420 [hep-ph]].
- [90] S. Dulat, T. J. Hou, J. Gao, M. Guzzi, J. Huston, P. Nadolsky, J. Pumplin, C. Schmidt, D. Stump and C. P. Yuan, “New parton distribution functions from a global analysis of quantum chromodynamics,” *Phys. Rev. D* **93**, no.3, 033006 (2016), [arXiv:1506.07443 [hep-ph]].
- [91] P. Jimenez-Delgado and E. Reya, “Dynamical NNLO parton distributions,” *Phys. Rev. D* **79**, 074023 (2009), [arXiv:0810.4274 [hep-ph]].
- [92] A. Accardi *et al.*, “Electron Ion Collider: The Next QCD Frontier : Understanding the glue that binds us all,” *Eur. Phys. J. A* **52**, no. 9, 268 (2016) [arXiv:1212.1701 [nucl-ex]].
- [93] P. Agostini *et al.* [LHeC Collaboration and FCC-he Study Group], “The Large Hadron-Electron Collider at the HL-LHC,” arXiv:2007.14491 [hep-ex].
- [94] A. Abada *et al.* [FCC Collaboration], “FCC Physics Opportunities : Future Circular Collider Conceptual Design Report Volume 1,” *Eur. Phys. J. C* **79**, no. 6, 474 (2019).
- [95] A. Abada *et al.* [FCC Collaboration], “FCC-hh: The Hadron Collider : Future Circular Collider Conceptual Design Report Volume 3,” *Eur. Phys. J. ST* **228**, no. 4, 755 (2019).